J. Appl. Comput. Mech., xx(x) (2026) 1-20
DOI: 10.22055/jacm.2026.49412.5958

ISSN: 2383-4536
jacm.scu.ac.ir

Shahid Chamran University of Ahvaz

Journal of Applied and Computational Mechanics

Research Paper

L-Shaped Stringer Tailoring to Enhance Axial Buckling of FGM Elliptical Cylindrical Shells

Davood Poorveis[1], Amin Khajehdezfuly[1], Shapour Moradi[2], Seyed Ali Emam[1]

[1] Department of Civil Engineering, Faculty of Civil Engineering and Architecture, Shahid Chamran University of Ahvaz, Ahvaz, Iran, Email: dpoorveis@scu.ac.ir (D.P.); amin_dezfuly@scu.ac.ir (A.Kh.); ali.em767676@gmail.com (S.A.E.)

[2] Department of Mechanical Engineering, Faculty of Engineering, Shahid Chamran University of Ahvaz, Ahvaz, Iran, Email: moradis@scu.ac.ir

Received May 26 2026; Revised August 27 2026; Accepted for publication September 05 2026.
✉ Corresponding author: D. Poorveis (dpoorveis@scu.ac.ir)

Abstract. A review of the literature indicates that buckling of longitudinal stiffeners is one of the primary challenges faced by stiffened cylindrical shells under axial compressive loads. In this study, conventional longitudinal stiffeners with rectangular cross-sections were replaced by innovative L-shaped stiffeners, aiming to enhance the structural stability of stiffened composite cylindrical shells. To demonstrate this concept, a functionally graded material (FGM) shell, an advanced form of composite with continuously varying properties, was modeled using the semi-analytical finite strip method in the FORTRAN environment. The results from the developed model were compared with those obtained from the finite element method to assess the model's accuracy. Through a comprehensive parametric study, the effects of shell geometry, L-shaped stiffener configuration, and the FGM power index on the axial buckling performance of the stiffened shell were investigated. The findings revealed that, for certain combinations of the investigated parameters, the axial buckling load of shells with L-shaped stiffeners can be approximately 40-70% higher than that of shells with conventional rectangular stiffeners, despite using the same material and stiffener cross-sectional area. This demonstrates that adopting alternative stiffener geometries provides a practical and effective strategy for enhancing the buckling resistance of composite structural shells in construction engineering applications.

Keywords: Functionally graded materials, Axial buckling, Stiffened elliptical cylindrical shell, L-shaped stiffener, Angle.

1. Introduction

Today, the use of thin-walled shells has developed in various industries for various reasons, such as their light weight. These structures, despite their low weight, have high resistance to various loads. A review of the literature shows that general or local buckling of thin-walled structures is the most common type of failure of these structures against external forces [1-3]. Accordingly, much research has been conducted on the effect of various parameters on the buckling of thin-walled shells [4, 5]. On the other hand, various researchers have proposed different methods to increase the buckling of these structures. Two of the most commonly used approaches to increase the buckling load the thin-walled structures are using non-isotropic materials (such as composite materials and Functionally Graded Materials (FGM) (as an advanced versions of composite materials)) to construct thin-walled structures [6-9] and using different types of stiffeners in the shell structures such as stringers (stiffeners utilized in longitudinal direction of the shell structure) and rings (stiffeners utilized in transversal direction of the shell structure) [10-12].

A review of the literature shows that there are several studies on the investigation of buckling of shell structures stiffened by different types of stiffeners [13]. For instance, Tian et al., [14] investigated the buckling behavior of ring-stiffened cylindrical shell subjected to general pressure loading using Ritz method and it was shown that the buckling load of the stiffened shell increases using proper distribution of ring stiffeners. Barani et al., [15] utilized Fourier-expansion based differential quadrature method to evaluate the effect of ring distribution on the buckling load of ring-stiffened laminated composite cylindrical shells. Fang et al., [16] investigated the influence of stiffeners on the free vibration characteristics of ring-stiffened elliptic cylindrical shells. Bai et al., [17] and Li et al., [18] indicated that the ring stiffeners have significant effects on the stability of ring-stiffened cylindrical shell and increase the buckling load the shell structure. Yang et al., [19] through a numerical study indicated that the buckling load of ring-stiffened composite shells is greater than that of unstiffened one. Rathinam et al., [20] investigated the buckling behavior of thin cylindrical shell stiffened by rings under external pressure. Li et al., [21] utilized artificial neural network to estimate the buckling load of non-uniformly ring-stiffened composite shells under hydrostatic pressure. Zhang et al., [22] experimentally and numerically studied the large-scale collapse of Titanium alloy ring-stiffened cylinder.

Published online: September 20 2026

As well as the ring, stringers, as stiffeners in longitudinal direction of the shell, are utilized for enhancing the buckling load of the structure. For instance, Chen et al., [23] studied the stability design of stringer-stiffened moderately-thick steel cylindrical shells under axial loads. Do et al., [24] investigated the ultimate strength of intact and defected steel stringer-stiffened cylinders under hydrostatic pressure. Kabir and Poorveis [25] evaluated the buckling of discretely stringer-stiffened composite cylindrical shells under combined axial compression and external pressure. Krasovsky and Kostyrko [26] performed an experimental study on the buckling of stringer-stiffened cylindrical shells under axial compression. Naghsh et al., [27] assessed the free vibration characteristics of stringer-stiffened general shells of revolution using a meridional finite strip method. Sadeghifar et al., [28] studied the buckling of stringer-stiffened laminated cylindrical shells with nonuniform eccentricity and indicated that the buckling of the structure increases by selecting an appropriate nonuniform distribution of eccentricity of stringers. Poorveis et al., [29] proposed an accurate approach for calculating the buckling load of stringer stiffened laminated composite cylindrical shells under axial compression. Ghorbanpour et al., [30] evaluated the buckling behavior of ring and stringer-stiffened cylindrical shells under general pressure and axial compression utilizing Ritz method. They indicated that ring and stringer stiffeners have significant effects on enhancement of buckling behavior of cylindrical shell. Yu and Qiao [31] developed an effective compound strip method for buckling analysis of stringer-, ring- or orthogonally-stiffened cylinders and investigated the number and depth of stiffeners on the buckling load of the structure.

A review of these studies shows that different characteristics of stiffeners, including their type, number, height, distribution, and material properties, can significantly affect the buckling resistance of stiffened shell structures. Beyond conventional longitudinal and ring stiffeners, several studies have investigated alternative stiffening concepts and advanced cylindrical shell configurations. For instance, Shahgholian-Ghahfarokhi and Rahimi [32] investigated the buckling behavior of grid-stiffened composite cylindrical shells under axial compression using the vibration correlation technique. Their study addressed the global buckling response of grid-stiffened cylindrical shells and demonstrated the importance of the stiffening architecture in determining the overall stability of the structure. In another study, Shahgholian-Ghahfarokhi and Rahimi [33] developed an analytical approach for the global buckling of composite sandwich cylindrical shells with lattice cores under uniaxial compression. Their results further demonstrated the contribution of the stiffening network to the global buckling resistance of cylindrical shell structures. In parallel with research on stiffened cylindrical shells, considerable attention has been devoted to the buckling behavior of functionally graded and advanced-material cylindrical shells. Shahgholian et al., [34] investigated the buckling response of functionally graded graphene-reinforced porous cylindrical shells using the Rayleigh–Ritz method, considering the effects of material gradation, porosity, graphene platelet distribution, and geometric parameters. Shahgholian-Ghahfarokhi et al., [35] further investigated the buckling of FG porous nanocomposite cylindrical shells reinforced with graphene platelets under uniform external lateral pressure. Their results demonstrated the significant influence of material distribution, porosity, reinforcement characteristics, and shell geometry on the buckling response

The above studies demonstrate that the buckling behavior of cylindrical shells is strongly influenced by both the stiffening architecture and the material and geometric characteristics of the shell. However, these two aspects have generally been investigated through different structural configurations: studies on grid- and lattice-stiffened shells have mainly focused on the effect of stiffening architecture on global stability, whereas studies on FGM and nanocomposite cylindrical shells have primarily examined material distribution, porosity, reinforcement characteristics, and shell geometry. These studies provide important insights into the buckling behavior of stiffened and advanced-material cylindrical shells, but they do not clarify how the cross-sectional geometry of an individual longitudinal stiffener affects the competition between local buckling of stiffener and global buckling of shell in an FGM elliptical cylindrical shell under axial compression. For conventional rectangular stiffeners, increasing the stiffener depth beyond a certain level can lead to premature local buckling of the stiffener before global buckling of the stiffened shell occurs. Consequently, further increasing the stiffener depth may not necessarily improve the overall buckling resistance of the shell and can even reduce the buckling load of the stiffened shell. This limitation motivates the consideration of L-shaped stiffeners, in which the flange can provide additional restraint to the web and delay its local buckling. For instance, Rodrigues et al., [36] showed that steel panels stiffened with T- and L-shaped (angle) stringers can achieve higher buckling loads than panels with rectangular stiffeners. Similarly, Elumalai et al., [37] demonstrated the significant influence of angle-shaped stiffeners on the buckling resistance of stiffened composite curved panels. These studies indicate that the cross-sectional configuration of a stiffener can affect the buckling response beyond the effect of simply increasing the amount of stiffener material. For a given stiffener cross-sectional area, an appropriate L-shaped configuration may therefore provide a greater increase in buckling resistance than a corresponding rectangular configuration. However, this potential benefit is not unlimited. Increasing either the web depth or the flange width of an L-shaped stiffener can itself increase the susceptibility of the stiffener components to local buckling. Therefore, the effects of the L-shaped stiffener geometry need to be systematically investigated to identify configurations that effectively enhance the axial buckling resistance without triggering premature local instability. Nevertheless, the available studies on angle-shaped stiffeners have mainly considered metallic panels or composite curved structures, while the interaction between L-shaped longitudinal stiffeners and an FGM elliptical cylindrical shell under axial compression remains insufficiently clarified. So, the specific scientific gap is the lack of a systematic understanding of how the cross-sectional geometry of longitudinal L-shaped stiffeners affects the competition between local stiffener buckling and global shell buckling in FGM elliptical cylindrical shells under axial compression. Previous investigations have generally examined stiffener architecture, advanced material characteristics, or non-rectangular stiffeners separately, and therefore have not established how the geometry of an individual longitudinal stiffener can be tailored to enhance shell buckling resistance while avoiding premature local stiffener buckling. Accordingly, this study investigates the axial buckling behavior of FGM elliptical cylindrical shells reinforced with longitudinal L-shaped stringers using a semi-analytical finite strip formulation. The principal objective is to clarify how the cross-sectional tailoring of the stiffener affects the buckling capacity and governing instability mode for a given stiffener cross-sectional area. So, this study goes beyond a simple comparison between rectangular and L-shaped stiffeners and focuses on the role of stiffener geometry in controlling the competition between local stiffener buckling and global shell buckling. The effects of the number of stringers, stiffener area index, total stiffener depth, angle ratio, shell aspect ratio, ellipse aspect ratio, and FGM power on buckling of stiffened shell are systematically examined. Particular attention is given to identifying the competing effects of stiffener depth and flange development and to determining the range of angle ratios that provides the most favorable buckling response within the investigated design space. To this end, a FORTRAN-based finite strip code was developed for the analysis of FGM elliptical cylindrical shells stiffened with L-shaped and rectangular stringers. The results obtained from the model developed in this study were validated against finite element results obtained using ABAQUS and against available results from the literature. A comprehensive parametric study was conducted to examine the effects of the stiffener and shell parameters on the axial buckling response.

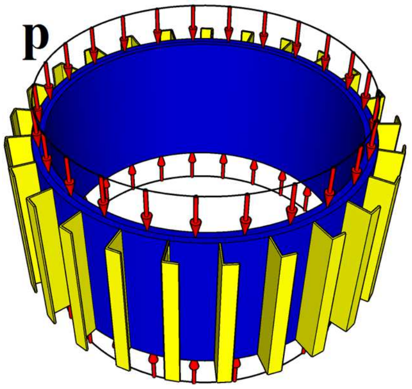

Fig. 1. Uniform axial compression applied to cylinder.

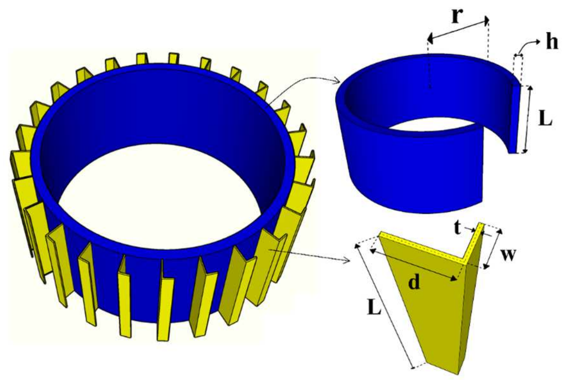

Fig. 2. Details of cylindrical elliptical shell stiffened by L-shaped stringers.

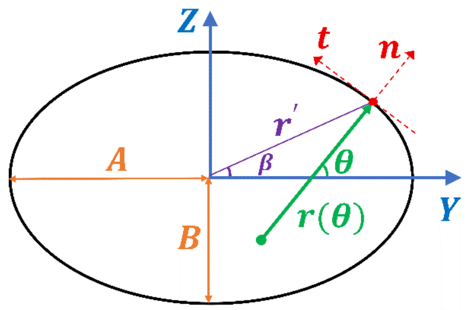

Fig. 3. Global and local coordinate systems considered for shell.

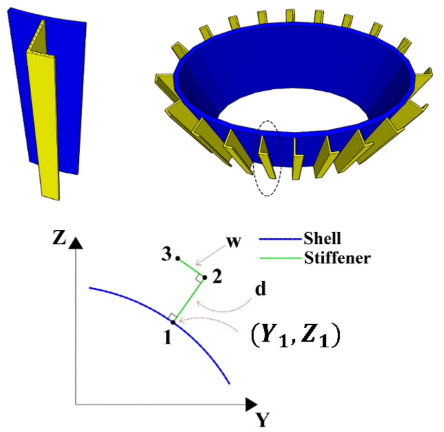

Fig. 4. geometry characteristics of L-shaped stiffener.

2. Numerical Model Development

In this study, a code was developed in FORTRAN environment to simulate the FGM elliptical cylindrical shell stiffened by L-shaped using semi-analytical finite strip method. Figure 1 shows a schematic view the FGM cylindrical elliptical shell stiffened by L-shaped subjected to uniform axial pressure (P) applied to leading and trailing edges of the simply supported shell. Figure 2 shows the details of FGM cylindrical elliptical shell stiffened by L-shaped. As presented in Fig. 2, h stands for the thickness of shell, L represents length of shell and stringers, t is thickness of L-shaped stiffener, d stands for the depth of L-shaped stiffener and w represents the width of L-shaped stiffener. In this study, $d+w$ and $d/(d+w)$ are entitled as "stiffener total depth" and "angle ratio", respectively. When the angle ratio is considered as 1, the stringer has a rectangular cross-section (entitled as conventional stiffener). As shown in Fig. 2, the stiffeners are uniformly distributed around the shell and the distance between them is the same.

Figure 3 presents global and local coordinate systems of the elliptical cylindrical shell considered in this study. As shown in this figure, Y and Z axes (as global coordinate system) are along the major and minor diameters of the ellipse, respectively. In this study, the major and minor radii of the ellipse are considered as A and B, respectively. According to Fig. 3, for an arbitrary point located on the ellipse, r' is central radius, β stands for central angle and θ is curvature angle and $r(\theta)$ represents curvature radius. The curvature radius $(r(\theta))$ and curvature angle (θ) are obtained by Eq. (1) and (2), respectively,

$$r(\theta)=\frac{A^2B^2}{(A^2\cos^2(\theta)+B^2\sin^2(\theta))^{3/2}} \tag{1}$$

$$\theta=\mathrm{Arc}\tan\left(\frac{A^2}{B^2}\tan(\beta)\right) \tag{2}$$

In addition, a normal-tangential coordinate system (as local coordinate system) was considered for each arbitrary point located on the ellipse (n-t local coordinate system). The geometry characteristics of L-shaped stringers are shown in Fig. 4.

The angle-shaped stringer has two legs. According to Fig. 4, the depth of angle-shaped stiffener is perpendicular to the shell edge. The width of angle-shaped stiffener is perpendicular to another leg of the stiffener. Each stiffener has three nodes, two of which are independent of the shell (nodes 1 to 3, as illustrated in Fig. 4). Node 1 is common between shell and stringer and accordingly, the coordinate of node 1 is determined based on the shell geometry (Y_1, Z_1). Displacement/rotation of other nodes of the stringer (nodes 2 and 3) are independent of the shell. Accordingly, Eqs. (3) and (4) provide the Z coordinates of nodes 2 and 3, respectively $(Z_2$ and $Z_3)$:

$$Z_2=m_{12}(Y_2-Y_1)+Z_1 \tag{3}$$

$$Z_3=m_{23}(Y_3-Y_2)+Z_2 \tag{4}$$

In Eqs. (3) and (4), Y_i stands for the Y coordinate of i-th node and Z_i is the Z coordinate of i-th node and m_{ij} represents the slope of the line between i-th and j-th nodes. As the depth leg of the stringer is perpendicular to the ellipse, m_{12} is the slope of the normal line on the ellipse. Moreover, as the width leg of the stringer is perpendicular to the depth leg, m_{23} is obtained using Eq. (5):

$$m_{23} = -\frac{1}{m_{12}} \tag{5}$$

Equation (6) calculates the distance between nodes 2 and 3, where d stands for the depth of stringer:

$$(Y_2 - Y_1)^2 + (Z_2 - Z_1)^2 = d^2 \tag{6}$$

Equation (7) was obtained by assembling Eqs. (3) and (6) to calculate Y_2 and accordingly, Eq. (8) presents the root of Eq. (7). Equation (8) presents the relationship between Y_1 and Y_2:

$$Y_2^{\,2}(1+m_{12})^2 - 2Y_2Y_1(1+m_{12}^{\,2}) + (Y_1^{\,2} + Y_1^{\,2}m_{12}^{\,2} - d^2) = 0 \tag{7}$$

$$(Y_2 - Y_1) = \pm\frac{d}{\sqrt{(1+m_{12}^{\,2})}} \tag{8}$$

The sign on the right side of Eq. (8) $(\pm)$ depends on sign of Y_1. For the positive and negative signs of Y_1, the sign on the right side of the equation is positive and negative, respectively. Same procedure was conducted to obtain the relationship between Y_2 and Y_3 (Eq. (9)):

$$(Y_3 - Y_2) = \pm\frac{w}{\sqrt{(1+m_{23}^{\,2})}} \tag{9}$$

The sign on the right side of Eq. (9) $(\pm)$ depends on sign of Z_2 which is obtained from Eq. (2). For the positive and negative signs of Z_2, the sign on the right side of the equation is negative and positive, respectively. The sign of m_{12} and m_{23} depends on the position of the stringers relative to the quadrants of the global coordinate system (Y-Z) of the ellipse. In the first and third quadrants, m_{12} is positive and m_{23} is negative. For the second and fourth quadrants, m_{12} is negative and m_{23} is positive. According to the ellipse Equation (Eq. 10), m_{12} and m_{23} were obtained. For this purpose, the derivative of any arbitrary point on the ellipse is calculated using Eq. (11) (by considering $Y_c = Z_c = 0$):

$$\frac{(Y - Y_c)^2}{A^2} + \frac{(Z - Z_c)^2}{B^2} = 1 \tag{10}$$

$$\frac{dZ}{dY} = -\frac{YB^2}{ZA^2} \tag{11}$$

Consequently, m_{12} and m_{23} are calculated using Eqs. (12) and (13), respectively,

$$m_{12} = \frac{Z_1A^2}{Y_1B^2} \tag{12}$$

$$m_{23} = -\frac{Y_1B^2}{Z_1A^2} \tag{13}$$

In this study, the FGM cylindrical elliptical shell stiffened by L-shaped stringers was discretized by several curved finite strip elements shown in Fig. 5. As illustrated in this figure, S stands for width of the strip element. Five degrees of freedom were considered on each node of strip element including u, v, w, φ_θ, and φ_x.

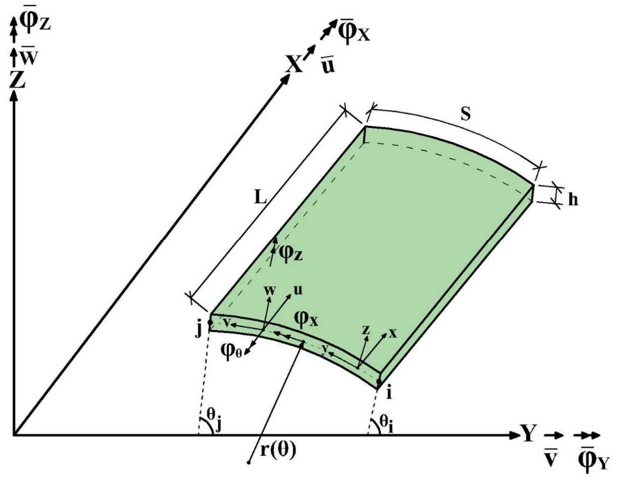

Fig. 5. Curved finite strip element considered in this study.

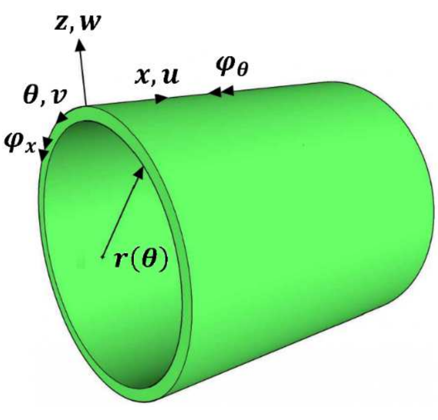

Fig. 6. 3D view coordinate system and degrees of freedom.

As shown in this figure, u, v, w, φ_θ, and φ_x are axial displacement in the longitudinal direction of the cylinder, displacement along the circumference of the cylinder, displacement in the radial direction of the cylinder, rotation about axial axis of cylinder and rotation about circumference direction of cylinder, respectively (Figs. 5 and 6). It should be noted that a local coordinate system was considered for the finite strip element (x, y, z) where y axis is along circumference direction of cylinder, x is along axial direction of cylinder and z is in the radial direction of the cylinder (Figs. 5 and 6). According to Fig. 5, two nodes (nodes i and j) were considered for estimating the shape function of strip element in the transverse direction of the element. In this study, the displacement of any arbitrary point of the shell ($\tilde{u}$, $\tilde{v}$ and $\tilde{w}$) was calculated according to the first-order shear deformation theory (Eq. (14)). All parameters utilized in Eq. (14) were defined earlier (Figs. 5 and 6):

$$\begin{aligned}\tilde{u}(x,\theta,z) &= u(x,\theta) + z\varphi_x(x,\theta)\\ \tilde{v}(x,\theta,z) &= v(x,\theta) + z\varphi_\theta(x,\theta)\\ \tilde{w}(x,\theta,z) &= w(x,\theta)\end{aligned} \tag{14}$$

In this research, Fourier series expansions and Lagrangian functions ($N_q(\eta)$, $\eta \in [-1,+1]$) were utilized to estimate the displacement functions in the longitudinal and transversal directions, respectively (Eq. (15)). In Eq. (15), p and q are the harmonic number in the longitudinal direction and the node number in the circumference direction, respectively. Referring to Eq. (15), displacement components at each node in the local coordinate system of each strip were approximated using a two-nodded curved strip interpolation in the circumferential direction and a Fourier series expansion in the longitudinal direction. To estimate the buckling load of the stiffened shell, two different stages, including pre-buckling and buckling analyses, were considered. In the pre-buckling phase, which consists of a static analysis under uniform axial load, several non-zero harmonic numbers (odd half-wave numbers) were used for the displacement components. Utilizing a sufficient number of harmonic terms ensures an accurate stress distribution between the shell and stringer strips, especially the membrane stresses required for the subsequent buckling analysis. Due to the presence of the second term in the u-component, the convergence rate in the pre-buckling stage is improved, and the need to use a larger number of harmonics is therefore reduced. In the current study, it was sufficient to use odd harmonics ranging from 1 to 11. In the buckling stage, due to the simply supported boundary conditions and the simplicity of the material properties over the lateral surfaces of the shell and stringers, each harmonic number was considered separately. Moreover, the second term in the u-component was neglected. In this stage, the harmonic number was varied from 1 to 30 in increments of 1, and the minimum buckling load was identified as the axial buckling load, while its corresponding harmonic number was taken as the longitudinal mode number of the stiffened shell. A longitudinal half-wave number of one indicates global buckling of the stiffened shell, without significant local buckling of the stringers. As the longitudinal half-wave number increases beyond one, the buckling response becomes increasingly associated with local buckling of the stringers, accompanied by negligible deformation of the shell skin. The corresponding buckling mode depends on the geometry and material properties of both the shell and stringers:

$$\begin{aligned}u &= \sum_{p=1}^{M}\sum_{q=1}^{2} u_{pq}\cos(\frac{p\pi}{L}x)N_q(\eta) + \sum_{q=1}^{2} u_{0q}N_q(\eta)(\frac{1}{2}-\frac{x}{L})\\ v &= \sum_{p=1}^{M}\sum_{q=1}^{2} v_{pq}\sin(\frac{p\pi}{L}x)N_q(\eta)\\ w &= \sum_{p=1}^{M}\sum_{q=1}^{2} w_{pq}\sin(\frac{p\pi}{L}x)N_q(\eta)\\ \varphi_x &= \sum_{p=1}^{M}\sum_{q=1}^{2} \varphi_{xpq}\cos(\frac{p\pi}{L}x)N_q(\eta)\\ \varphi_\theta &= \sum_{p=1}^{M}\sum_{q=1}^{2} \varphi_{\theta pq}\sin(\frac{p\pi}{L}x)N_q(\eta)\end{aligned} \tag{15}$$

In folded-plate structures, unlike conventional plate structures, the DOFs associated with different strips along a common nodal line may have different orientations according to the local coordinate system of each strip. Therefore, to assemble the stiffness matrices of individual strips and form the global structural stiffness matrix (**K**), it is necessary to transform the DOFs of each strip from its local coordinate system to the global coordinate system. In the present study, for both the pre-buckling and buckling analyses, the degrees of freedom of the shell and stringers are transformed to the global X–Y–Z coordinate system. Referring to Fig. 5, for strip i–j, the following matrix relation holds:

$$\bar{\Delta}^k = T\Delta^k \tag{16}$$

where, k is strip number and $\bar{\Delta}^k$ and Δ^k are defined as:

$$\begin{aligned}\bar{\Delta}^k &= [\bar{\Delta}_i, \bar{\Delta}_j]^T\\ \Delta^k &= [\Delta_i, \Delta_j]^T\end{aligned} \tag{17}$$

in which, $\bar{\Delta}_i$ and Δ_i vectors in global and local systems, respectively, are as follows:

$$\begin{aligned}\bar{\Delta}_i &= [\bar{u}_i, \bar{v}_i, \bar{w}_i, \bar{\varphi}_{x_i}, \bar{\varphi}_{\theta_i}, \bar{\varphi}_{z_i}]\\ \Delta_i &= [u_i, v_i, w_i, \varphi_{x_i}, \varphi_{\theta_i}, \varphi_{z_i}]\end{aligned} \tag{18}$$

It should be noted that, in the present investigation, each strip has five DOFs at each node in the local coordinate system. Accordingly, a drilling DOF (ϕ_z) has been added at each node to facilitate a consistent transformation from the local to the global coordinate system. Furthermore, the local stiffness matrix is augmented with zero entries in the rows and columns corresponding to these additional DOFs. Moreover, the transformation matrix, T, for a two-nodded strip can be defined as follows:

$$T = \begin{bmatrix} T_i & 0 \\ 0 & T_j \end{bmatrix} \tag{19}$$

in which, 6×6 square matrix T_i is as follows:

$$T_i = \begin{bmatrix} 1 & 0 & 0 & 0 & 0 & 0 \\ 0 & \cos\bar{\theta}_i & \sin\bar{\theta}_i & 0 & 0 & 0 \\ 0 & \sin\bar{\theta}_i & -\cos\bar{\theta}_i & 0 & 0 & 0 \\ 0 & 0 & 0 & 0 & -1 & 0 \\ 0 & 0 & 0 & \cos\bar{\theta}_i & 0 & \sin\bar{\theta}_i \\ 0 & 0 & 0 & \sin\bar{\theta}_i & 0 & -\cos\bar{\theta}_i \end{bmatrix} \tag{20}$$

Referring to Fig. 5, for the shell strips $\bar{\theta}_i = \theta_i + \pi/2$ and the stringer strips $\bar{\theta}_i = \theta_i$, interchanging i and j leads to the following form T_j. Based on the invariance of strain energy under a change of coordinate system, the following relation holds for the stiffness matrix in the global coordinate system, $\bar{\mathrm{K}}$, and the corresponding stiffness matrix in the local coordinate system, k:

$$\bar{\mathrm{K}} = \mathrm{T}k\mathrm{T}^{\mathrm{T}} \tag{21}$$

Equation (22) presents the generalized strain vector ($[\varepsilon]$) considered in this research:

$$[\varepsilon]^{\mathrm{T}} = [\varepsilon_{xx}, \varepsilon_{\theta\theta}, \gamma_{x\theta}, k_{xx}, k_{\theta\theta}, k_{x\theta}, \gamma_{xz}, \gamma_{\theta z}] \tag{22}$$

In Eq. (22), ε_{xx}, $\varepsilon_{\theta\theta}$, $\gamma_{x\theta}$, k_{xx}, $k_{\theta\theta}$, $k_{x\theta}$, γ_{xz} and $\gamma_{\theta z}$ are normal strain of middle plane in x direction, normal strain in θ direction, shear strain in $x\theta$ plane, bending curvature about θ direction, bending curvature about x direction, torsional curvature in $x\theta$ plane, xz plane shear strain in the shell thickness direction and θz plane shear strain in the shell thickness direction, respectively. The linear and nonlinear terms of different components of strain vector were obtained based on the Sanders theory and are available in the literature [38-39]. Equation (23) presents the relationship between generalized stress and strain vectors [6]:

$$\begin{Bmatrix} N_{xx} \\ N_{\theta\theta} \\ N_{x\theta} \\ M_{xx} \\ M_{\theta\theta} \\ M_{x\theta} \\ Q_{xz} \\ Q_{\theta z} \end{Bmatrix} = \begin{bmatrix} A_{11} & A_{12} & A_{16} & B_{11} & B_{12} & B_{16} & 0 & 0 \\ A_{12} & A_{22} & A_{26} & B_{12} & B_{22} & B_{26} & 0 & 0 \\ A_{16} & A_{26} & A_{66} & B_{16} & B_{26} & B_{66} & 0 & 0 \\ B_{11} & B_{12} & B_{16} & D_{11} & D_{12} & D_{16} & 0 & 0 \\ B_{12} & B_{22} & B_{26} & D_{12} & D_{22} & D_{26} & 0 & 0 \\ B_{16} & B_{26} & B_{66} & D_{16} & D_{26} & D_{66} & 0 & 0 \\ 0 & 0 & 0 & 0 & 0 & 0 & H_{44} & H_{45} \\ 0 & 0 & 0 & 0 & 0 & 0 & H_{45} & H_{55} \end{bmatrix} \begin{Bmatrix} \varepsilon_{xx} \\ \varepsilon_{\theta\theta} \\ \gamma_{x\theta} \\ k_{xx} \\ k_{\theta\theta} \\ k_{x\theta} \\ \gamma_{xz} \\ \gamma_{\theta z} \end{Bmatrix} \tag{23}$$

The vector in the left side of Eq. (23) stands for the generalized stress vector of any arbitrary point placed at the middle surface of the cylinder. In Eq. (23), N_{xx}, $N_{\theta\theta}$, $N_{x\theta}$, M_{xx}, $M_{\theta\theta}$, $M_{x\theta}$, Q_{xz} and $Q_{\theta z}$ stand for normal membrane force per unit length in x direction, normal membrane force per unit length in θ direction, in-plane shear stress in $x\theta$ plane, bending moment per unit length about θ direction, bending moment per unit length about x direction, torsional moment per unit length in $x\theta$ plane, out of xz plane force per unit length in the shell thickness direction and out of θz plane shear force per unit length in the shell thickness direction, respectively. Moreover, A_{ij}, B_{ij}, D_{ij} and H_{ij} are ith and jth components of axial, axial-flexural, flexural and out of plane shear rigidity matrices, respectively and are obtained from Eq. (24):

$$\begin{aligned} (A_{ij}, B_{ij}, D_{ij}) &= \int_h (1, z, z^2)\bar{Q}_{ij}(z)dz \qquad i,j = 1,2,6 \\ H_{ij} &= K_s \int_h \bar{Q}_{ij}(z)dz \qquad i,j = 4,5 \end{aligned} \tag{24}$$

In Eq. (24), K_s is shear correction factor and was considered as 5/6. Moreover, $\bar{Q}_{ij}(z)$ represents i-th and j-th components of reduced stiffness matrix and is calculated using Eq. (25). It should be noted that for the FGM material, $\bar{Q}_{16}$, $\bar{Q}_{26}$ and $\bar{Q}_{45}$ are zero:

$$\begin{aligned} \bar{Q}_{11} &= \bar{Q}_{22} = \frac{E(z)}{1-\upsilon(z)^2} \\ \bar{Q}_{12} &= \bar{Q}_{21} = \frac{\upsilon(z)E(z)}{1-\upsilon(z)^2} \\ \bar{Q}_{44} &= \bar{Q}_{55} = \bar{Q}_{66} = \frac{E(z)}{2(1+\upsilon(z))} \end{aligned} \tag{25}$$

In Eq. (25), $E(z)$ and $\upsilon(z)$ are modulus of elasticity and Poisson ratio of material in depth of z, respectively. In this study, the cylinder was made of FGM (Fig. 7). As shown in Fig. 7, the shell material properties change gradually along the shell thickness, from material properties 1 to those of material 2. Accordingly, Eqs. (26) and (27) were utilized for calculating the modulus of elasticity and Poisson ratio of FGM in depth of z_i ($E(z_i)$ and $\upsilon(z_i)$), where, subscripts m and c refer to the metal and ceramic properties, respectively. Moreover, $V_c(z_i)$ is volumetric ratio of ceramic in depth of z_i [6, 7] and is obtained using Eq. (28):

$$E(z_i) = (E_c - E_m) \times V_c(z_i) + E_m \tag{26}$$

$$\upsilon(z_i) = (\upsilon_c - \upsilon_m) \times V_c(z_i) + \upsilon_m \tag{27}$$

$$V_c(z_i) = (\frac{z_i}{h} + \frac{1}{2})^N \tag{28}$$

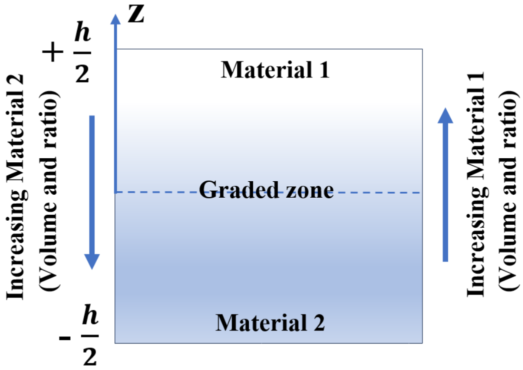

Fig. 7. variation of material properties in FGM along shell thickness.

In Eq. (28), N stands for the power of FGM and is a positive number. In this research, the Poisson's ratio is constant (υ = 0.21). In this study an FGM shell consisting of a ceramic inner layer $(E_c = 151000\ \text{N/mm}^2)$ and a metal outer layer $(E_m = 70000\ \text{N/mm}^2)$ is considered. Moreover, all isotropic stiffeners are assumed to be made of metal.

In this study, elastic stiffness matrix (K_E) of the strip element in the global coordinate system was obtained based on the virtual internal work $(\delta W_{\text{int}}^{\text{lin}})$ performed by linear terms of virtual strains $(\{\varepsilon^L\})$ and their corresponding generalized stresses (Eq. (29)):

$$\delta W_{\text{int}}^{\text{lin}} = \int_x \int_\theta (N_{xx}\delta\varepsilon_{xx}{}^L + N_{\theta\theta}\delta\varepsilon_{\theta\theta}{}^L + N_{x\theta}\delta\gamma_{x\theta}{}^L + M_{xx}\delta k_{xx}{}^L + M_{\theta\theta}\delta k_{\theta\theta}{}^L + M_{x\theta}\delta k_{x\theta}{}^L + Q_{xz}\delta\gamma_{xz}{}^L + Q_{\theta z}\delta\gamma_{\theta z}{}^L) r(\theta) d\theta dx \tag{29}$$

So, the elastic stiffness matrix for j-th strip element and the shell $([K_{E_j}]$ and $K_E)$ were obtained from Eq. (30):

$$\delta W_{\text{int}}^{\text{lin}} = \sum_{j=1}^{nstrip} (\delta\bar{\Delta}^j)^T \left[K_{E_j}\right] \bar{\Delta}^j = (\delta\bar{\Delta})^T K_E \bar{\Delta} \tag{30}$$

In Equation (30), $\bar{\Delta}^j$ is displacement/rotation vector of j-th strip element in global coordinate system and $\bar{\Delta}$ is displacement/rotation vector of the shell in the global coordinate system (X, Y, Z). The external virtual work performed by uniform axial pressure applied to edges of the cylinder $(\delta W_{\text{ext}}^{sh})$ was obtained using Eq. (31) to extract the external force vector of the shell ({F}):

$$\delta W_{\text{ext}}^{sh} = \int_{-1}^{+1} \bar{P}_{sh} \left[\sum_{p=1}^{M}\sum_{q=1}^{2} \delta u_{pq} N_q(\eta)(1-\cos(p\pi)) + \sum_{q=1}^{2} \delta u_{0q} N_q(\eta)\right] J\, d\eta \tag{31}$$

In Eq. (31), J is Jacobian determinant between global and local coordinate systems. Equation (31) was simplified as Eq. (32). In Eq. (26), $F_{pq,sh}^u$ and $F_{0q,sh}^u$ coefficients are obtained using Eq. (33):

$$\delta W_{\text{ext}}^{sh} = \sum_{p=1}^{M}\sum_{q=1}^{2} \delta u_{pq}^{sh} F_{pq,sh}^u + \sum_{q=1}^{2} \delta u_{0q}^{sh} F_{0q,sh}^u \tag{32}$$

$$\begin{aligned} F_{pq,sh}^u &= \int_{-1}^{+1} \bar{P}_{sh}\, N_q(\eta)(1-\cos(p\pi)\, J\, d\eta \\ F_{0q,sh}^u &= \int_{-1}^{+1} \bar{P}_{sh}\, N_q(\eta)\, J\, d\eta \end{aligned} \tag{33}$$

The internal virtual work done by virtual nonlinear terms of membrane strains $(\delta\varepsilon_{xx}{}^{nl},\ \delta\varepsilon_{\theta\theta}{}^{nl}$ and $\delta\gamma_{x\theta}{}^{nl})$ and their corresponding membrane stresses (N_{xx}^0 , $N_{\theta\theta}^0$ and $N_{x\theta}^0$) were obtained using Eq. (34) for extracting the geometric stiffness $([K_G])$:

$$\delta W_{\text{int}}^{nlin} = \int_x \int_\theta (N_{xx}^0 \delta\varepsilon_{xx}{}^{nl} + N_{\theta\theta}^0 \delta\varepsilon_{\theta\theta}{}^{nl} + N_{x\theta}^0 \delta\gamma_{x\theta}{}^{nl}) r(\theta) d\theta dx \tag{34}$$

A pre-buckling analysis was performed to obtain the initial displacement of the shell subjected to a unit uniform axial pressure. The initial membrane forces $(N_{xx}^0,\ N_{\theta\theta}^0$ and $N_{x\theta}^0)$ were obtained from the pre-buckling analysis [40]. Therefore, the geometric stiffness matrix for j-th strip element and the shell in the global coordinate system $([K_{G_j}]$ and $K_G)$ were obtained from Eq. (35):

$$\delta W_{\text{int}}^{nlin} = \sum_{j=1}^{nstrip} (\delta\bar{\Delta}^j)^T \left[K_{G_j}\right] \bar{\Delta}^j = (\delta\bar{\Delta})^T K_G \bar{\Delta} \tag{35}$$

Finally, the eigenvalues (λ) and mode shape vector (ϕ) of the stiffened FGM elliptical cylindrical shell (Eq. (36)):

$$(K_E - \lambda K_G)\phi = 0 \tag{36}$$

3. Convergence and Validation of Model

In this section, the convergence and validation of the results obtained from the numerical model developed in this study were evaluated through two steps. The details are provided in the following sub-sections.

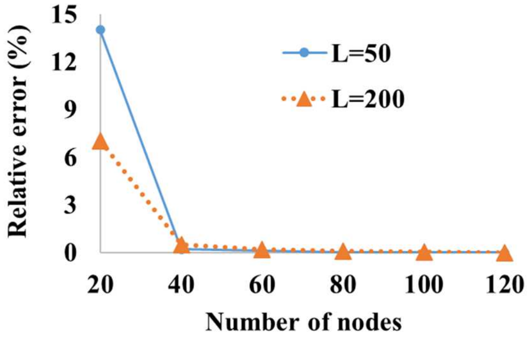

Fig. 8. Effect of number of nodes (strip elements) on convergence of model.

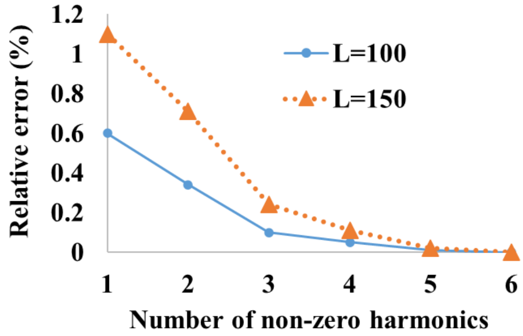

Fig. 9. Effect of number of harmonics on convergence of model.

3.1. Model convergence

According to the literature, as the number of strip elements and harmonics increases, the accuracy of the results and computational cost of the finite strip model increase. Therefore, an appropriate number of harmonics and elements should be determined to achieve results with appropriate accuracy while taking into account low computational cost. Consequently, the effect of variation of number of strip elements and harmonics on the convergence of results obtained from the model was assessed. In this regard, an isotropic cylindrical shell with a circular cross-section, radius of 100 mm, and thickness 1 mm stiffened by 10 angle-shaped stringers and subjected to axial compressive load was considered in this section. The depth and width of angle stiffeners are 16 and 4 mm, respectively. The Young's modulus and Poisson's ratio of the shell were considered as 2000 N/mm^2 and 0.3, respectively. The effect of variation of number of strip elements (nodes) on relative error is shown in Fig. 8. In Fig. 8, two values are considered for the length of the shell (50 and 200 mm) and number of harmonics is 6 (odd numbers 1 to 11). It is evident that for the shells with lengths of 50 and 200 mm, the buckling load converges with the increase in the number of nodes in the shell circumference for different lengths. As shown in Fig. 8, as the number of nodes increases from 20 to 120, the relative error decreases significantly. However, when the number of nodes exceeds 80, the convergence of the model reaches an acceptable level. For investigation of the effect of number of harmonics on the convergence of the model, the length of the shell was considered as 100 and 150 mm. Moreover, the number of stringers increased to 30 angle-shaped stiffeners. The effect of variation of number of harmonics on relative error is shown in Fig. 9. As illustrated in Fig. 9, as the number of odd harmonics increases from 1 to 11, the relative error decreases significantly. However, when the harmonic number exceeds 9, the convergence of the model reaches an acceptable level.

To assess the effect of using a greater number of nodes (DOFs) in the web of the L-shaped stiffener, some stringer-stiffened FGM cylinders were analyzed. The shell cross-section was selected to be circular (B / A = 1), and the L / R ratio was 0.5, 1.0, 1.5, and 2.0. The shell thickness was set to 1.0 mm, and an L-shaped stiffener was considered. The angle ratio of the L-shaped stringer was set to 0.7, and the total depth of the stringers ($d + w$), was 16 and 20 mm. The FGM power indices were $N = 0$ and $N = 2$. Moreover, the shell skin was modeled using 64 curved two-nodded strips, and the total number of stringers was fixed at 32 in all cases. The stringers were modeled using either two or three straight strips. The longitudinal half-wave number was varied from 1 to 30, and for each half-wave number, an eigenvalue buckling analysis under a uniform axial load was performed to determine the minimum buckling load. Stringer area index is 20%. Tables 1 and 2 summarize the results for different stringer models (two-strip and three-strip models). The longitudinal half-wave numbers are presented in parentheses in Tables 1 and 2. The longitudinal half-wave number was 1 for all cases except one. For L / R = 0.5 and an FGM power index of 2, the three-strip model exhibited a local buckling mode with four half-waves along the cylinder length. The differences between the two discretization models for L / R = 0.5 were larger than those observed for the other length-to-radius ratios. Moreover, an increase in the total depth of the L-shaped stringer resulted in a greater difference in the predicted axial buckling loads between the two discretization models considered in the analyses. Furthermore, the results indicate that an increase in the FGM power index reduces the difference between the two discretization approaches.

To further assess the capability of the developed model to capture changes in the buckling mode, particularly the transition from global shell buckling to local stringer buckling, an additional parametric analysis was performed. An elliptical cylindrical shell subjected to axial compression was discretized using 96 two-nodded curved strips for the shell skin and 32 rectangular stingers simulated with two strip elements. The cylinder was assumed to be isotropic, with $E = 2000$ N/mm^2 and $\upsilon = 0.3$, and the length-to-equivalent-radius ratio was set to $L / R_0 = 1$. The stringer height was varied from 5 to 14 mm in increments of 1 mm, while three minor-to-major radius ratios, B / A = 0.5, 0.7, and 1.0, were considered. Stringer area index was 20% and shell thickness was considered as 1 mm. Under axial compression, a pre-buckling static analysis was first performed, with the applied axial load distributed between the shell and stringers according to their respective axial stiffnesses. The corresponding buckling loads, optimum stringer heights, and longitudinal half-wave numbers are summarized in Table 3. As presented in Table 3, increasing the stringer height initially increases the buckling load of the stiffened shell, as the stringers carry a greater portion of the axial membrane load. However, beyond a certain stringer height, the buckling load decreases, accompanied by an increase in the longitudinal half-wave number. This change in the governing half-wave number indicates a transition from global buckling of the stiffened shell to local buckling of the stringers, demonstrating the capability of the developed finite-strip model to capture different buckling modes and their dependence on stringer geometry and shell aspect ratio. The results therefore provide an additional verification of the model's ability not only to predict the buckling load but also to identify changes in the governing buckling mode under different geometric configurations.

Based on the convergence results presented above, the discretization and harmonic parameters adopted in the subsequent analyses were selected to provide an appropriate balance between numerical accuracy and computational efficiency. Accordingly, the shell skin was discretized using 120 two-nodded curved strip elements, while each rectangular and L-shaped stringer was represented by two and three strip elements, respectively. In the pre-buckling stage, a static analysis was performed under the applied axial load, with the harmonic terms considered simultaneously. Owing to the symmetry of the loading and its invariance along the longitudinal direction of the cylinder, only odd harmonics contribute to the pre-buckling response. The second term in the u-displacement component improves the convergence rate of the pre-buckling solution and reduces the number of harmonic terms required.

Table 1. Effect of L-shaped stringer discretization on buckling load of stiffened elliptical cylindrical shell (N/mm) for a total stringer depth of d + w = 16 mm.

FGM power index	Stringer discretization	$L / R_0 = 0.5$	$L / R_0 = 1$	$L / R_0 = 1.5$	$L / R_0 = 2$
0	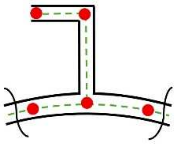	2170.815 (1)	1250.935 (1)	1031.071 (1)	939.137 (1)
0	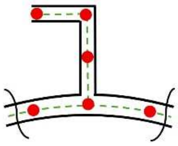	2118.856 (1)	1252.584 (1)	1026.658 (1)	939.137 (1)
2	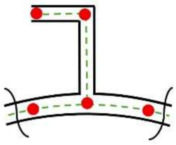	1761.809 (1)	924.280 (1)	708.108 (1)	627.363 (1)
2	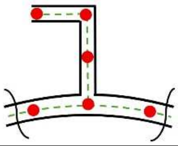	1722.452 (1)	918.869 (1)	704.455 (1)	624.727 (1)

Table 2. Effect of L-shaped stringer discretization on buckling load of stiffened elliptical cylindrical shell (N/mm) for a total stringer depth of $d + w$ = 20 mm.

FGM power index	Stringer discretization	$L / R_0 = 0.5$	$L / R_0 = 1$	$L / R_0 = 1.5$	$L / R_0 = 2$
0	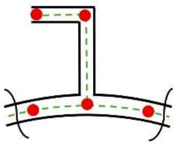	2573.781 (1)	1462.501 (1)	1128.426 (1)	989.179 (1)
0	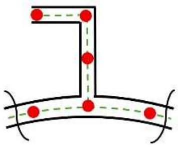	2461.152 (1)	1451.706 (1)	1122.701 (1)	984.825 (1)
2	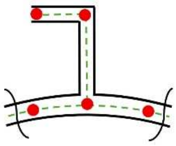	2159.630 (1)	1107.113 (1)	797.966 (1)	675.152 (1)
2	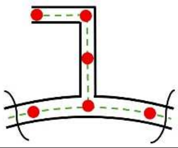	1880.232 (4)	1097.722 (1)	793.092 (1)	671.470 (1)

Table 3. Effect of rectangular stringer depth on buckling load (N/mm) and longitudinal half-wave number of stiffened elliptical cylindrical shell.

hst	B / A		
	0.5	0.7	1.0
5	7.365 (1) *	10.429 (1)	13.457 (1)
6	7.787 (1)	10.725(1)	13.677 (1)
7	8.347 (1)	11.181 (1)	14.090 (1)
8	9.003 (1)	11.773 (1)	14.661 (1)
9	9.735 (1)	12.460 (1)	15.360 (1)
10	10.513 (1)	13.220 (1)	16.162 (1)
11	11.314 (1)	14.029 (1)	16.097 (6)
12	12.126 (1)	14.148 (14)	14.147 (14)
13	12.509 (14)	12.252 (14)	-
14	10.976 (15)	-	-
(hst)opt	12.80	11.76	10.57
(Pcr)max	12.767 (1)	14.657 (1)	16.655 (1)

* Number in parentheses indicates longitudinal half wave number

Table 4. Properties of stiffened shell.

E (N/mm^2)	υ	L (mm)	R (mm)	h (mm)	A_{st} / A_{sh} (%)	$d + w$ (mm)	d / ($d + w$)
2000	0.3	100	100	1	30	12	0.8

Table 5. Difference between buckling loads obtained from finite strip model and ABAQUS.

Number of stringers	Buckling load (N/mm)		Difference between buckling loads (%)
	Finite element model (ABAQUS)	Finite strip model (This study)	
20	13.64	13.35	2.1
40	20.3	19.76	2.67

Accordingly, odd harmonic numbers from 1 to 11 were adopted in the subsequent parametric analyses. In the buckling stage, the second term in the -displacement component was neglected. Moreover, for the adopted material properties and boundary conditions, the coupling terms A_{16}, A_{26}, B_{16}, B_{26}, D_{16} and D_{26} vanish. Consequently, the harmonic terms are decoupled, allowing each harmonic number to be considered independently. The harmonic number was therefore varied from 1 to 30 with an increment of 1, and the minimum buckling load among the considered harmonics was taken as the axial buckling load of the stiffened shell, with its corresponding harmonic number representing the longitudinal half-wave number. These discretization and harmonic settings, together with the adopted treatment of the second term in the u-displacement component, were subsequently maintained throughout the parametric analyses.

3.2. Model validation

The validation of the numerical model developed in this study was conducted in two stages. First, the results obtained from the model were compared with those obtained from a finite element model developed in ABAQUS software. Second, the numerical results obtained from the model were compared with analytical and experimental results reported in the previous studies.

3.2.1. Numerical validation

A comparison was made between the results obtained from the model developed in this study and those obtained from the numerical model developed in ABAQUS software to evaluate the validity of the results obtained from the model. In this regard, a circular cylindrical shell stiffened by angle-shaped stringers was developed in the ABAQUS software (as commercial finite element software). The stiffened shell was modeled using 4360 S8R5 elements. The S8R5 element is an eight-node quadrilateral shell element with reduced integration, suitable for the analysis of thin and moderately thick shell structures and capable of accounting for both membrane and bending deformation. In the numerical model developed in this study, the shell skin was discretized using 120 two-nodded curved finite-strip elements. One Gauss integration point located at the center of each strip was employed for numerical integration. Each rectangular and L-shaped stringer was modeled using two and three strip elements, respectively. The properties of the stiffened shell are presented in Table 4. In this table, A_{st} / A_{sh} stands for the ratio of stiffeners area (A_{st}) to the shell edge area (A_{sh}). The thickness of the stiffener and the shell is assumed to be the same. In order to more accurately evaluate the effect of angle-shaped stiffeners on the accuracy of the model, two different values (inducing 20 and 40) were considered for the number of stiffeners (Fig. 10). Table 5 presents the buckling loads obtained from the model developed in this study and those calculated by ABAQUS.

As presented in Table 5, there is minor difference between the results obtained from the model developed in this study and those calculated by ABAQUS (less than 3%). It shows that the model developed in this study has an acceptable accuracy on calculating the buckling load of cylindrical shell stiffened by angle-shaped stringer under axial pressure.

3.2.2. Analytical and experimental validation

Almroth [41] investigated the buckling load of cylinder under axial compression using an analytical approach (entitled as smeared stiffness model). Furthermore, Abramovich et al., [42] experimentally evaluated the buckling load of a cylindrical shell subjected to lateral pressure. Table 6 indicates geometry and material properties of these isotropic stringer-stiffened cylinders analyzed under uniform axial compression and lateral pressure [41, 42]. In this table, n_{st} represents number of uniformly spaced rectangular stringers in each case. Furthermore, A_1 is stringer cross-section area, b_1 is the distance between two consecutive stiffeners and e_1 denotes stringer eccentricity relative to the shell middle surface. Accordingly, the shell considered in reference [41] was modelled in this study by 120 curved two-nodded strips along with 60 two-nodded straight strips. Moreover, to model cylindrical shell in case C2, 168 curved two-nodded strips for shell skin and 84 two-nodded straight strips for stringers have been applied in this study. Table 7 Compares the results of buckling of two cases, C1 and C2, obtained by analytical (smeared stiffness model) and experimental methods, respectively with the current results. Due to different modellings and discretization, agreement of the results is acceptable.

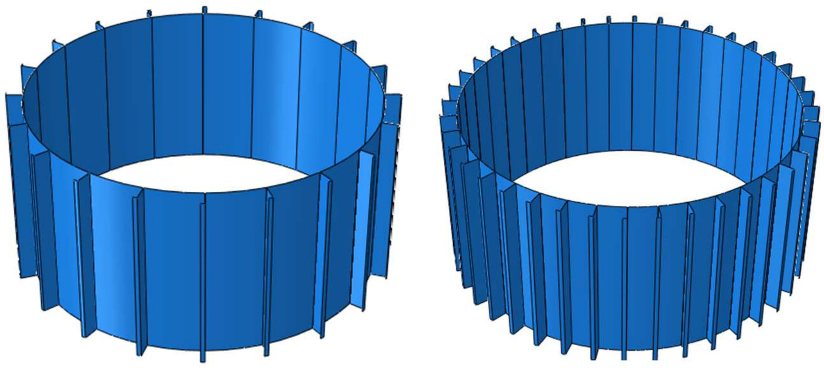

(a) (b)

Fig. 10. Cylindrical shell stiffened by different numbers of angle-shaped stringers; (a) 20, (b) 40.

Table 6. Outside stringer-stiffened cylindrical shells dimensions (E = 7500 kg/mm^2, υ = 0.3).

Reference	Case	Shell length (mm)	Radius (mm)	Thickness (mm)	n_{st}	$(A_1 / b_1 h)$	(e_1 / h)
[41]	C1	965.20	242.57	0.719	60	1.028	5.830
[42]	C2	200.00	120.27	0.249	84	0.666	4.030

Table 7. Comparison experimental and analytical results with the buckling loads obtained from this study.

Case	Approach	Type of loading	Unit of buckling load	Results reported in previous study	Results calculated in this study	Difference (%)
C1	Analytical	Axial Compression	kg/mm	20.43	21.42	4.85
C2	Experimental	Lateral Pressure	kg/mm^2	0.001355	0.001249	7.82

Table 8. Parameters considered in parametric study.

Parameter	Values	Unit
Stringer area index $((A_{st} / A_{sh}) \times 100)$	10, 20, 30	%
Number of stringers (N_{st})	20, 30, 40	-
Total depth of stringer ($d + w$)	8, 10, 12, 14, 16, 18, 20	mm
Angle ratio ($d / (d + w)$)	0.6, 0.7, 0.8, 0.9, 1	-
Shell length (L)	50, 100, 150, 200	mm
Ratio of major to minor diameters of ellipse (B / A)	0.6, 0.7, 0.8, 0.9, 1	-
Power of FGM (N)	0, 0.5, 1, 2, 10, 100	-

4. Parametric Study

A parametric study was conducted to investigate the effect of L-shaped stiffeners on axial buckling of a simply supported FGM elliptical cylindrical shell. As presented in Table 8, different values were considered for several effective parameters on buckling load of stiffened shell (including ratio of stiffeners area to the shell edge area ($100 \times A_{st} / A_{sh}$) (which is designated as stringer area index), number of stringers (N_{st}), total depth of stringer cross-section ($d + w$), angle ratio ($d / (d + w)$), shell length (L), ratio of minor to major radii of ellipse (B / A) and power of FGM (N)) through the parametric study. It should be noted that an isotropic circular cylindrical shell stiffened by 30 stringers having stringer area index of 30%, angle ratio of 0.8 and stiffener total depth of 14 mm was considered as the reference model ($N = 0$, B / A = 1, $N_{st} = 30$, $(A_{st} / A_{sh}) \times 100 = 30$, $d / (d + w) = 0.8$ and $d + w = 14$). In the reference model, thickness of shell, length of the shell and radius of shell were 1, 100 and 100 mm, respectively (h = 1 mm, L = 100 mm, R = 100 mm). It should be noted that the elliptical cross-sections considered for different ratios have the same perimeter, allowing the effect of the ratio on the buckling response to be evaluated under a constant-perimeter condition. In this regard, the dimensions of all elliptical sections (B and A) examined in this section were considered in such a way that the perimeter of all elliptical sections was equivalent to the perimeter of a circular section with a radius of 100 mm. It is worth mentioning that when the angle ratio is 1, the stringer has a rectangular cross-section (entitled as conventional stiffener). The results obtained from the parametric study are provided in the following sub-sections.

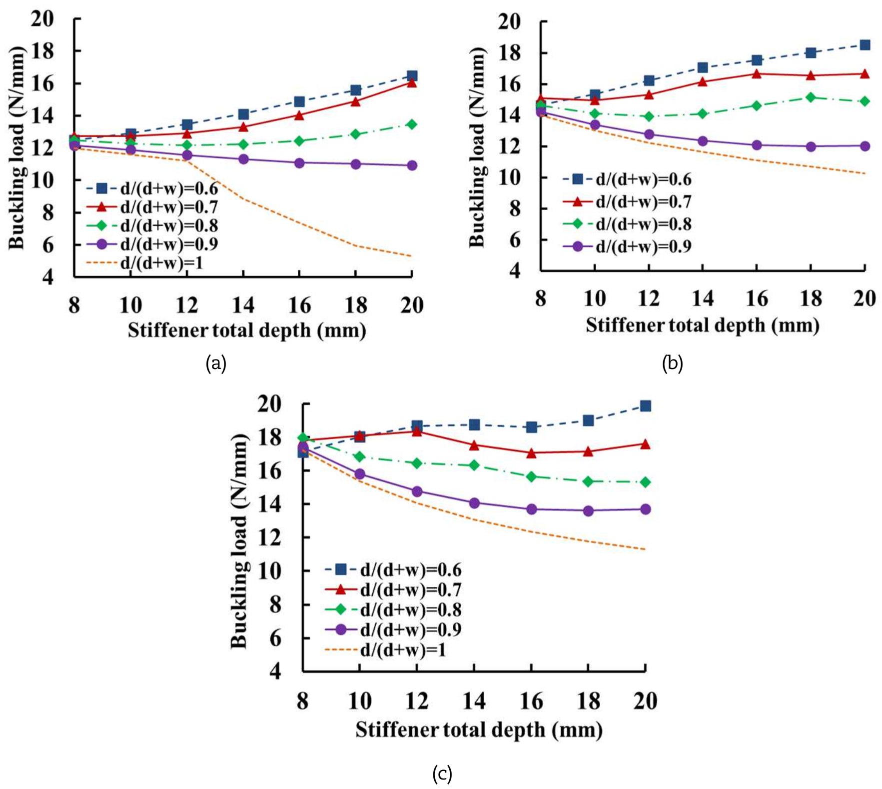

Fig. 11. Effect of stiffener total depth on buckling load of shell stiffened by 20 stringers by considering different stringer area indices; (a) 10%, (b) 20%, and (c) 30%.

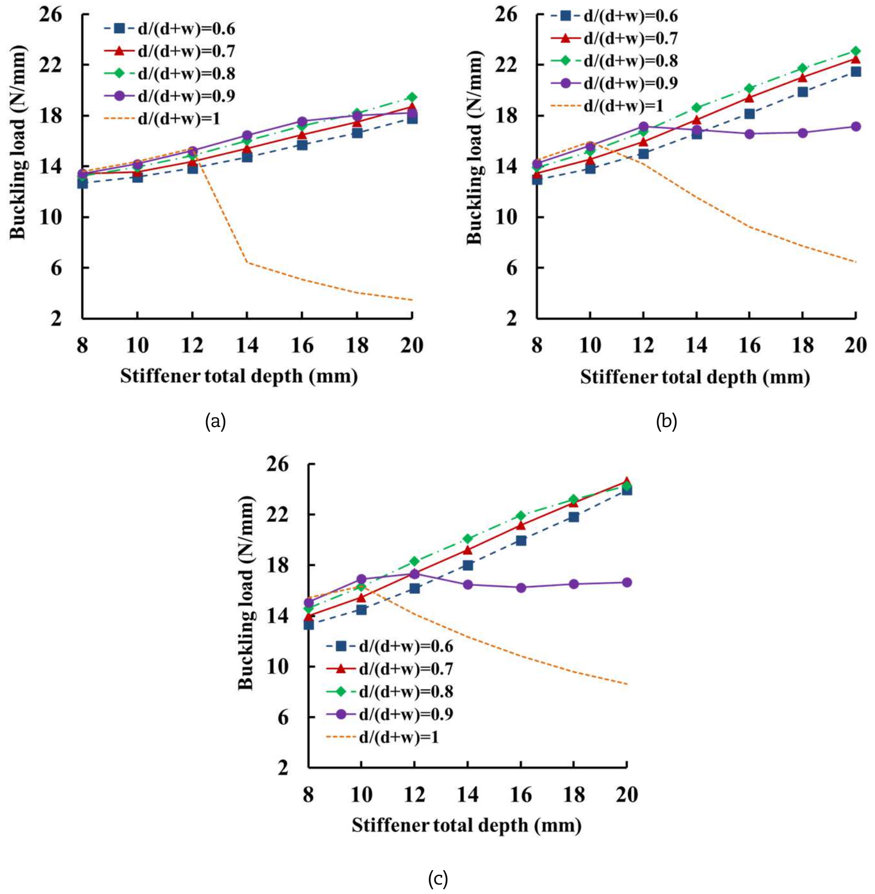

Fig. 12. Effect of stiffener total depth on buckling load of shell stiffened by 30 stringers by considering different stringer area indices, (a) 10%, (b) 20%, and (c) 30%.

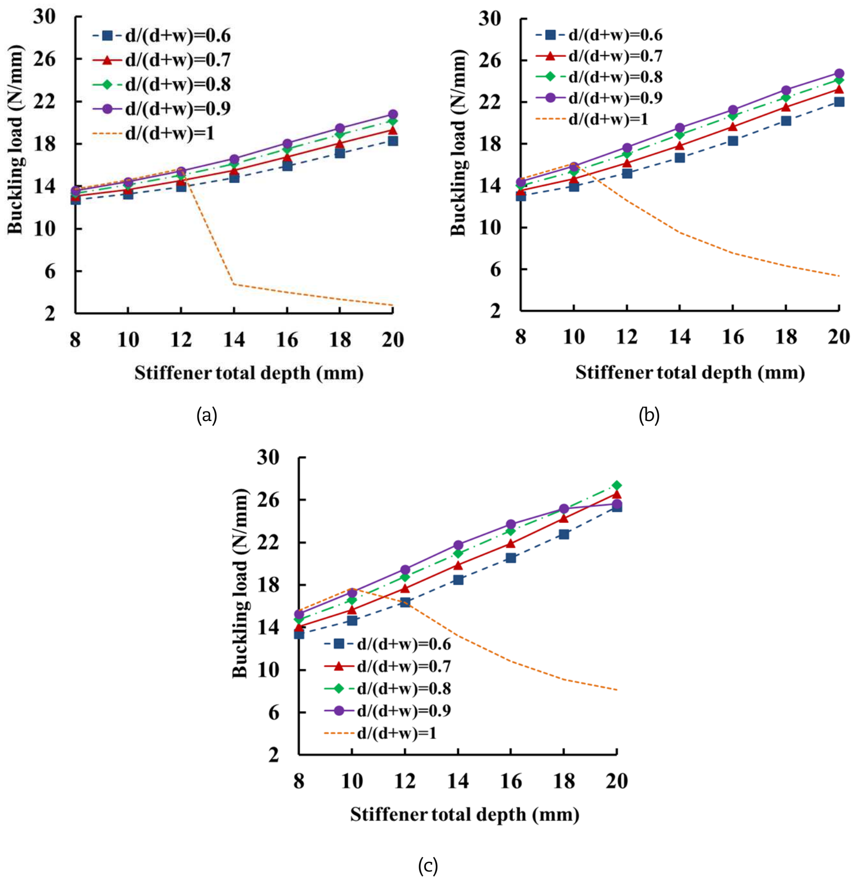

Fig. 13. Effect of stiffener total depth on buckling load of shell stiffened by 40 stringers by considering different stringer area indices, (a) 10%, (b) 20%, and (c) 30%.

4.1. Effect of stiffener properties on buckling load

In this section, the effect of variation of stringer area index, stiffener total depth and number of stringers on the buckling load of the shell was investigated. In this section, an isotropic circular cylindrical shell with radius and length of 100 mm (B / A = 1 and L = 100 mm) and a thickness of 1 mm was considered. Figures 11 to 13 show the effect of total depth of stringer, number of stringers and angle ratio on buckling load of the shell.

In Figs. 11 to 13, for 20, 30, and 40 stiffeners, the use of angle-shaped stiffeners results in a significant improvement in the shell's buckling load. However, when the number of stiffeners is large and the total depth of stiffener is short, the L-shaped stiffeners have a negligible effect on enhancing the buckling load. In other words, the influence of L-shaped stiffeners on improving the buckling load is most pronounced when the number of stiffeners is small or its total depth is large. The reason for this behavior is related to the characteristics of the conventional stiffener (with a rectangular cross-section). As shown in these figures, when the depth of the conventional stiffener exceeds a certain threshold (approximately 10 to 12 mm), the buckling load of the shell stiffened with this type of stiffener decreases significantly. This is because the boundary conditions of different edges of a conventional: both the upper and lower edges are simply supported, one side is free, and the other side is connected to the shell skin. When the stiffener total depth exceeds a certain range, its excessive slenderness leads to local buckling of the stiffener, occurring before the general buckling of the stiffened shell. This is clearly illustrated in Fig. 11, where the number of stiffeners is small (20) and each stiffener is subjected to relatively high axial loads. In this case, increasing the depth of the conventional stiffener from 8 mm to 12, 14, and 20 mm results in reductions of approximately 8, 30, and 42 percent in the shell's buckling load, respectively. In contrast, when the number of conventional stiffeners is moderate or high (30 and 40) and each stiffener carries a lower load, as shown in Figs. 12 and 13, increasing the stiffener total depth up to a certain range (10–12 mm) increases the buckling load by about 12–20%. In these cases, the buckling load of the shell reinforced with conventional stiffeners is only slightly higher than that of a shell with angle-shaped stiffeners. However, when the stiffener total depth exceeds this range, the stiffener slenderness becomes excessive, leading to local buckling of the conventional stiffener before global buckling of the shell. Under these conditions, the buckling load of the shell with L-shaped stiffeners is significantly higher than that of the shell reinforced with conventional stiffeners.

The reason for this lies in the functional differences between a conventional stiffener (with a rectangular cross-section) and an angle-shaped stiffener. The key distinction is the addition of a vertical leg (referred to as the "width") at the end of the conventional stiffener (in case of angle-shaped stiffener), accompanied by a reduction in its depth. In the L-shaped stiffener, the depth of the conventional stiffener is redistributed between the "width" and "depth" legs. The width leg acts like a simply supported beam, increasing the stiffener's bending stiffness. However, because the total depth of the L-shaped stiffener is fixed, increasing its width necessarily reduces its depth, which in turn decreases its bending stiffness. Due to these two opposing effects on the bending stiffness and slenderness of angle-shaped stiffener, there exists an optimal angle ratio that maximizes the buckling load of the stiffened shell. This optimal ratio depends on several parameters, including the number of stiffeners, the stiffener area percentage, the shell length, and the stiffener total depth.

When the number of stiffeners is 20 (Fig. 11), the spacing between them is large, and each stiffener carries a significantly higher share of the axial compressive load compared to the cases with 30 or 40 stiffeners. As a result, both the stiffeners and the shell body become more susceptible to local buckling. In this case, as shown in Fig. 11, although any increase in the depth of a conventional stiffener reduces the buckling load, increasing the total depth of an angle-shaped stiffener with an angle ratio of 0.6 raises the shell's buckling load at low and medium stringer area indices (10% and 20%), leading to an improvement of about 25% in the buckling load. Furthermore, as the stringer area index increases, the buckling load of the stiffened shell increases in all cases (Fig. 11).

When the number of stiffeners is 30 or 40 (Figs. 12 and 13), replacing conventional stiffeners with angle-shaped stiffeners leads to a substantial improvement in the buckling load. As shown in Figs. 12 and 13, the higher the stringer area index and angle ratio, the greater the improvement in the shell's buckling load. For example, when the number of stiffeners is 30, the stringer area index is 30%, and the stiffener total depth is 20 mm, the buckling load of the shell stiffened with angle-shaped stiffeners having angle ratios of 0.9, 0.8, 0.7, and 0.6 increases by about 266%, 252%, 231%, and 216%, respectively, compared to the shell with conventional stiffeners. As an interesting point in these cases, a same volume of material is utilized for both conventional and L-shaped stiffeners. This highlights the significant influence of stiffener geometry on enhancing its performance and increasing the buckling load of the stiffened shell. As shown in Figs. 12 and 13, for stiffeners with large aspect ratios (such as 0.9 and 0.8), when the stiffener total depth exceeds a certain threshold (about 10 to 18 mm for an angle ratio of 0.9, and more than 18 mm for an angle ratio of 0.8), the buckling load of the shell begins to decrease with further increases in the stiffener total depth. In these cases, the higher the stringer area index, the shorter the total depth at which this decreasing trend appears. For large angle ratios, the width of the angle is relatively small, which means that, at large stiffener total depths, there is still a risk of local buckling in the stiffener. This is clearly visible in the mode shapes shown in Figs. 14 and 15. Figure 14 illustrates the first buckling mode shapes of a shell stiffened by 30 stringers with an angle ratio of 0.9, stiffener total depth of 14 mm, and different stringer area indices.

Moreover, Fig. 15 presents the effect of varying the number of stiffeners on the first buckling mode shapes of the shell. As shown in Fig. 14, the global buckling occurs when the stringer area index is 10% (Fig. 14(a)). However, when the stringer area index is 20% or 30% (Figs. 14(b) and 14(c)), the excessive slenderness of the stiffeners causes local buckling of the stiffeners only, with no significant deformation in the shell skin. Similarly, as shown in Fig. 15, for 30 stiffeners (Fig. 12) with a stringer area index of 30% and an angle ratio of 0.9, local buckling occurs in the stiffeners, and not in the shell skin, when for different stiffener total depths (12, 14, or 18 mm). When the number of stiffeners is small (20), the 0.6 angle-shaped stiffener provides a greater improvement in the shell's buckling load compared to the other options (Fig. 11). In this case, increasing the total depth of the L-shaped stiffener from 8 to 20 mm (Fig. 11) raises the buckling load by approximately 7% to 35%. However, this rate of increase diminishes as the stringer area index grows. The buckling load achieved with the 0.6 L-shaped stiffener is higher than that of the conventional stiffener, and the difference between them widens with increasing stiffener total depth. For example, when the stiffener total depth increases from 8 to 20 mm, the buckling load of the shell reinforced with the 0.6 L-shaped stiffener is about 2% to 166% greater than that of the shell reinforced with the conventional stiffener, respectively. In contrast, an examination of the results in Figs. 12 and 13 (30 and 40 stiffeners) shows that increasing the total depth of the angle-shaped stiffener from 8 to 20 mm, with an angle ratio of 0.8, consistently increases the shell's buckling load by about 35% to 85%. In these cases, the buckling load of the shell reinforced with a 0.8 L-shaped stiffener is considerably higher than that of the shell with a conventional stiffener; for example, increasing the stiffener total depth from 10 to 20 mm raises the buckling load by approximately 25% to 225%, respectively.

4.2. Effect of shell length on buckling load

In this section, the effect of shell length on the buckling load of isotropic circular cylindrical shells with radius of 100 and thickness of 1 mm stiffened by 30 stiffeners (having stringer area index of 30%) is investigated (Fig. 16). It is evident from Fig. 16 that as the length of the cylindrical shell increases, the buckling load decreases for each total depth of stiffener, regardless the value of angle ratio. With increasing the total depth of stiffener, the buckling load increases or remains constant at any length of the shell, but for the conventional stiffener (angle ratio of 1), increasing its depth leads to decrease the buckling load of the shell.

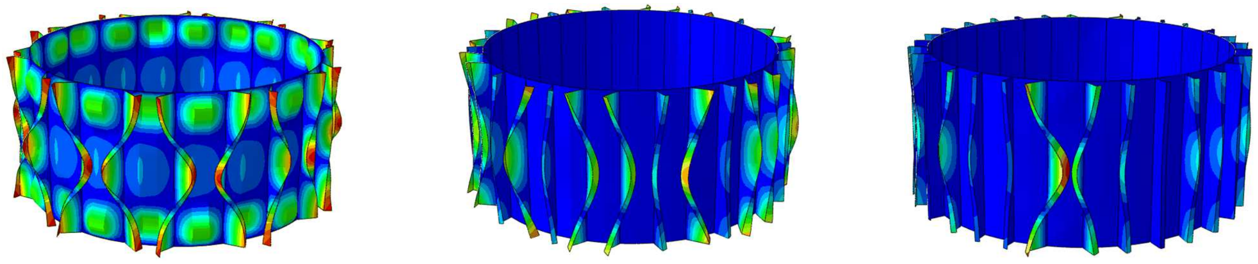

(a) (b) (c)

Fig. 14. Effect of stringer area index on first mode shapes of shell having 30 stringers with total depth of 14 mm and angle ratio of 0.9; (a) 10%, (b) 20%, and (c) 30%.

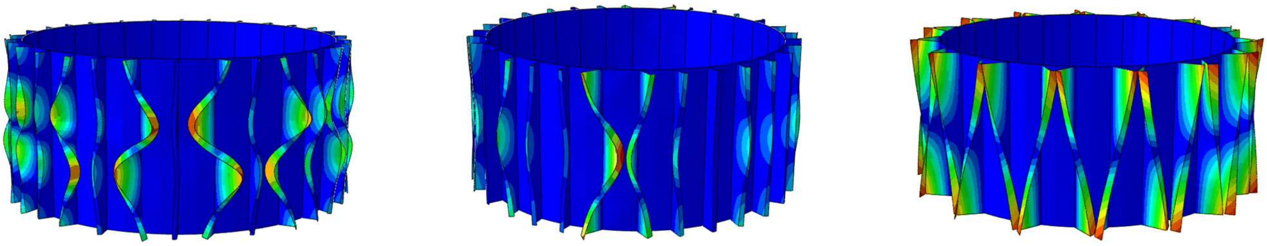

(a) (b) (c)

Fig. 15. Effect of total depth of stiffener on first mode shapes of shell stiffened by 30 stringers (having stringer area index of 30% and angle ratio of 0.9); (a) 12, (b) 14, and (c) 18.

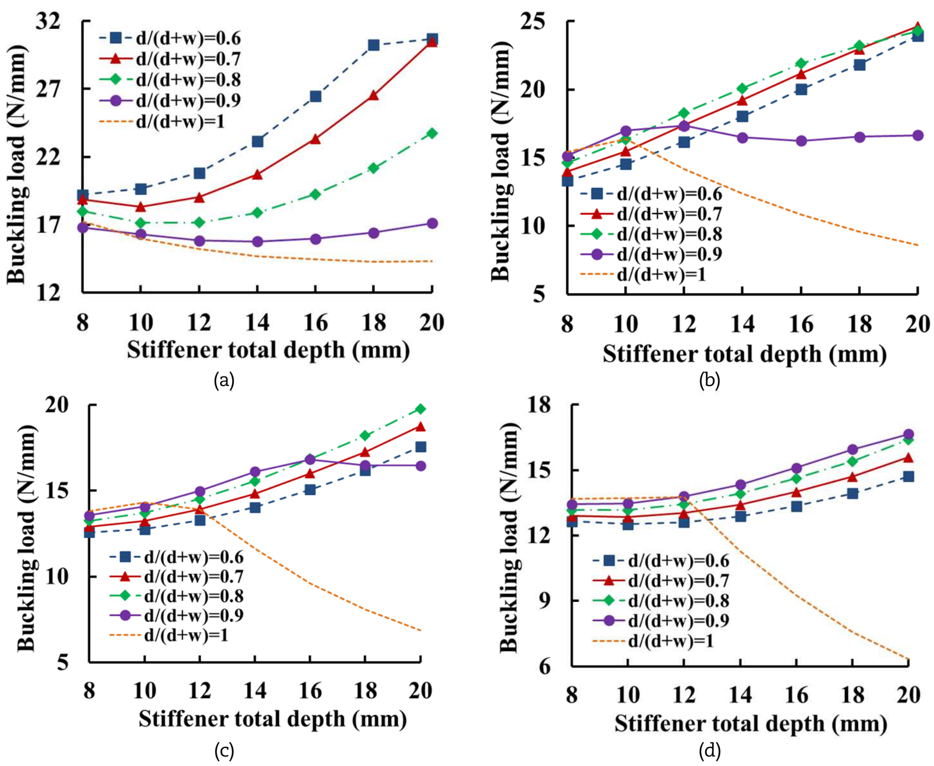

Fig. 16. Effect of shell length on buckling load of circular cylindrical shell stiffened having 30 stringers with 30% stringer area index; (a) 50 mm, (b) 100 mm, (c) 150 mm, and (d) 200 mm.

For the short shells, increasing the total depth of stiffener and reducing its thickness increase the difference between buckling loads of the stiffened shell equipped with different angle ratios. When the shell length is short (50), reducing the angle ratio does not significantly decrease the slenderness of the angle-shaped stringer. For the short shell, a lower angle ratio achieves a higher buckling load, and the conventional stiffener gives the lowest buckling load compared to the angle stiffeners. Accordingly, an angle-shaped stiffener with a ratio of 0.6 performs best in this case. Moreover, as the stiffener total depth or cross-section increases, the buckling load of the short shell also increases. Regardless of the results obtained for the short shell with a length of 50, the overall trend observed in Fig. 16 is consistent with that in Figs. 12 and 13. As the shell length increases, the buckling load of the shell decreases. For the long shell (L = 200), an increase in the stiffener total depth leads to a higher buckling load across all angle ratios. However, for shells with lengths of 100 and 150, this increasing trend is observed only for angle ratios below 0.9. On average, the improvement in the buckling load of shells stiffened with L-shaped stringers (with angle ratio less than 0.8) is approximately 59%, 52%, 46%, and 20% for shell lengths of 50, 100, 150, and 200, respectively. This indicates that as the shell length increases, the influence of L-shaped stringers on enhancing the buckling load diminishes.

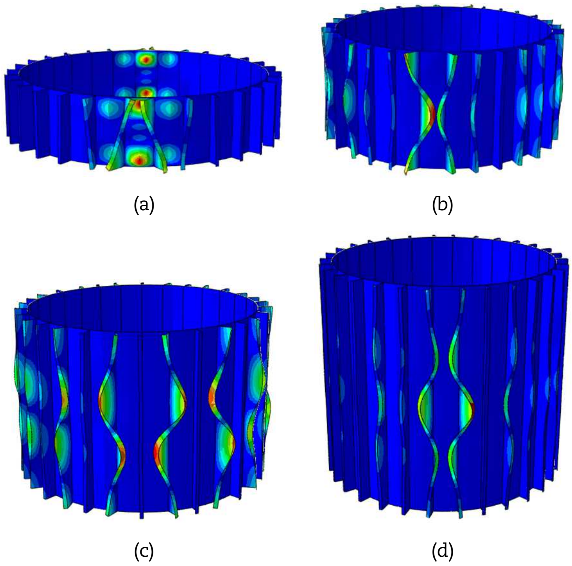

Fig. 17. Effect of shell length on first mode shapes of stiffened shell by 30 stringers having stringer area index of 30%, total depth of 20 mm and angle ratio of 0.9; (a) 50, (b) 100, (c) 150, and (d) 200.

Nevertheless, in all cases the buckling load of shells stiffened with L-shaped stringers remains higher than that of shells stiffened with conventional stiffeners, with improvements ranging from about 20% to 150%. Figure 17 illustrates the effect of shell length on the first mode shapes of a stiffened shell reinforced with 30 stringers, characterized by a stringer area index of 30%, a total depth of 20 mm, and an angle ratio of 0.9. While the shell and stringers are buckled in Fig. 17(a) (shell length of 50 mm), only stiffeners are locally buckled in Figs. 17(c) to 17(d) (the shell is not buckled in these cases). For shell lengths of 100 to 200 mm (Figs. 17(b) to 17(d)), the stiffener has taken a wavy shape, and with the increase in the length of the shell, the number of buckling half-waves has increased.

4.3. Effect of ovalization of cross-section on buckling load

In this section, the effect of cross-sectional ovalization (ellipticity) on the buckling load of a shell stiffened with angle-shaped stringers is investigated. It should be noted that as the ratio B/A decreases, the cross-section of the shell becomes more elongated and oval, whereas as B/A increases, the cross-section more closely resembles a circle. An elliptical cross-section with a perimeter equal to that of a circle of radius 100 mm is considered. The shell thickness is assumed to be 1 mm, and the cylinder is stiffened with 30 stringers. In addition, the stringer area index is taken as 30%. Figure 18 illustrates the effect of cross-sectional ovalization on the buckling load of the stiffened shell.

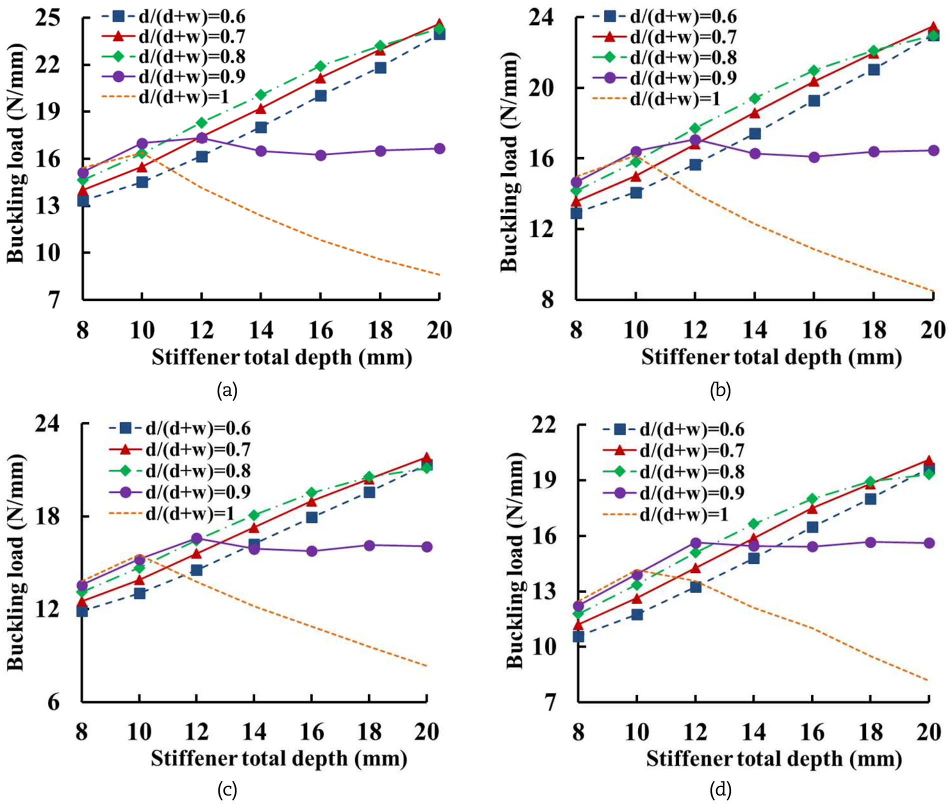

Fig. 18. Effect of B/A on buckling load of shell stiffened by 30 stringers having stringer area index of 30%; (a) 1, (b) 0.9, (c) 0.8, (d) 0.7, and (e) 0.6.

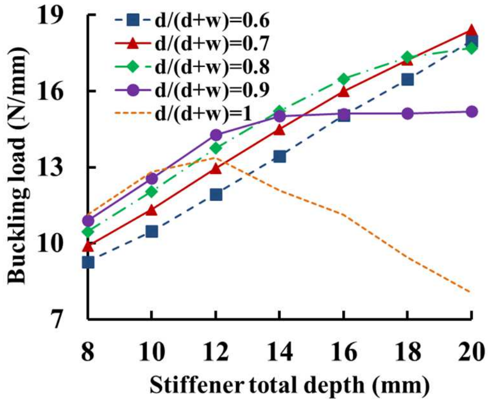

(e)

Fig. 18. Continued.

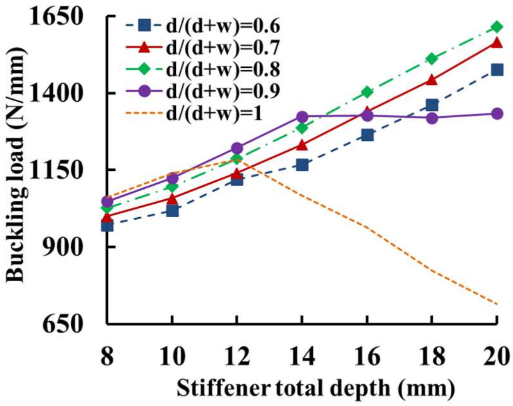

(a)

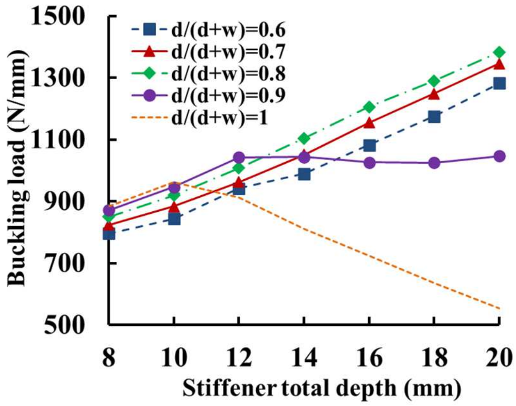

(b)

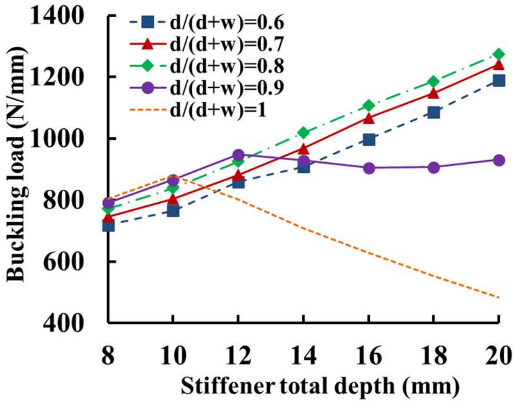

(c)

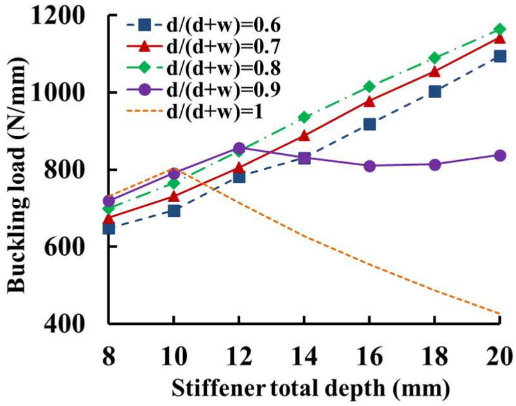

(d)

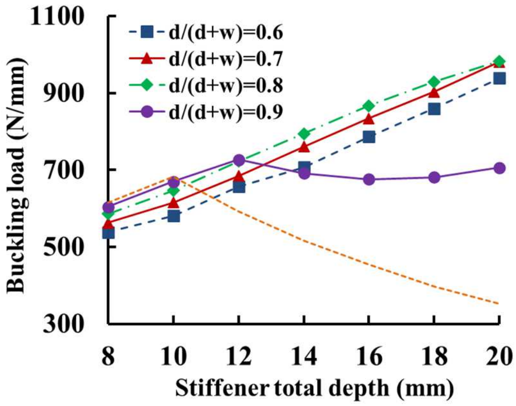

(e)

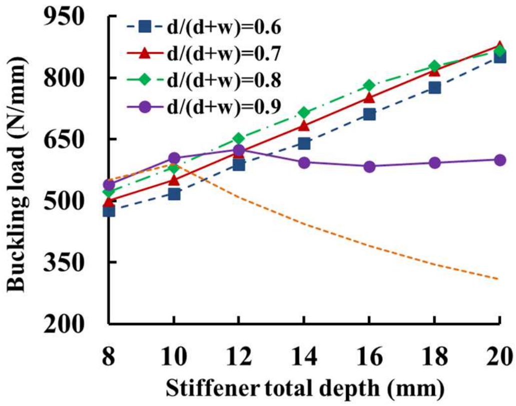

(f)

Fig. 19. Effect of FGM power on buckling load of shell stiffened by 30 stringers having stringer area index of 30%; (a) 0, (b) 0.5, (c) 1, (d) 2, (e) 10, and (f) 100.

According to Fig. 18, as the shell cross-section changes from a circle to an ellipse (i.e., as the B / A ratio decreases), the buckling load of the shell stiffened with either L-shaped or conventional stiffeners decreases, while the overall patterns of the results presented in Figs. 18(a) to 18(e) remain relatively similar. For instance, the buckling loads of the shell stiffened with stringers of 14 mm total depth and an angle ratio of 0.8 are 8.20, 19.41, 18.08, 16.63, and 15.21 N/mm for B / A values of 1, 0.9, 0.8, 0.7, and 0.6, respectively. These results clearly demonstrate the gradual decrease in buckling load with decreasing B / A. It should also be noted that the reduction in B / A does not significantly affect the relative influence of the L-shaped stiffeners on the buckling load of the shell. When the total depth of the L-shaped stiffener is 20, the average increases in the buckling load of the stiffened shell with B / A ratios of 1, 0.9, 0.8, 0.7, and 0.6 are 65%, 76%, 62%, 72%, and 68%, respectively (for stiffeners with an angle ratio less than 0.9). When the stiffener total depth is reduced to 14, the corresponding increases in buckling load are 30%, 38%, 39%, 45%, and 50%. These results indicate that the use of L-shaped stiffeners (with an angle ratio less than 0.9) in elliptical shells with any B/A ratio can enhance the buckling load by up to approximately 60%.

4.4. Effect of FGM power on buckling load

In this section, the FGM power index is taken as 0, 0.5, 1, 2, 10, and 100. The buckling load of an FGM circular cylindrical shell with a radius of 100 mm and a thickness of 1 mm, stiffened by 30 stringers with a stringer area index of 30%, is evaluated in this section (Fig. 19). A comparison of the results obtained for different FGM powers (Figs. 19(a) to 19(f)) shows that variation in the FGM power has no significant effect on the influence of the L-shaped stiffener in improving the buckling load of the FGM shell. In other words, the trend of the buckling load of the stiffened shell with respect to changes in stiffener total depth and angle ratio remains the same for all FGM powers. This indicates that the relative advantage of the L-shaped stiffener over the conventional rectangular stiffener is largely maintained across the investigated range of FGM power indices. However, the FGM power itself has a considerable effect on the buckling load of the stiffened shell. When the FGM power is zero, the shell is entirely ceramic, and as the FGM power increases, the rate of transition from ceramic to metal through the shell thickness also increases. At high FGM powers (e.g., $N = 100$), the shell becomes entirely metallic. Consequently, the buckling load of the shell decreases slightly with increasing FGM power in all cases.

Therefore, although the FGM power index affects the absolute buckling load, it does not substantially alter the effectiveness of the L-shaped stiffener within the investigated parameter range. As Figs. 19(a) to 19(f) demonstrate, an increase in the FGM power index (N), leads to a decrease in the axial buckling capacity of all stringer-stiffened elliptical cylindrical shells, regardless of the type of stringer used (i.e., rectangular or L-shaped). Based on the FGM power-law distribution given in Eqs. (26) and (28), $N = 0$ corresponds to a fully ceramic shell, for which the modulus of elasticity is nearly twice that of the metal constituent used in the FGM. As N increases, the ceramic-to-metal transition through the shell thickness becomes more rapid, and the effective modulus of elasticity of the shell decreases, resulting in a reduction in the buckling capacity of the stiffened shell. Another important point is the role of the stringers in enhancing the buckling capacity of the stiffened shell. The modulus of elasticity of the stringers is equal to that of the metal constituent of the FGM. Therefore, an increase in the FGM power index (N), changes the relative stiffness between the shell and the stringers, thereby affecting the contribution of the stringers to the overall buckling capacity of the stiffened shell. As N increases, this relative stiffness effect becomes more pronounced.

4.5. Comparison between performances of rectangular and L-shaped stringers

The objective of this section is to compare the effects of rectangular and L-shaped stringers on the buckling load of the stiffened shell. In addition, the influence of stringer cross-sectional configuration on the longitudinal half-wave number of the buckled stiffened shell is investigated. The results presented in Table 9 compare buckling loads of rectangular and L-shaped stringer-stiffened elliptical FGM cylindrical shells. The model consists of 64 curved two-nodded strips for the shell skin, together with 32 uniformly spaced external stringers. Each rectangular stringer is modeled using 2 strips, whereas each L-shaped stringer is modeled using three two-nodded strips. An FGM power index of $N = 2$ was considered for the shell skin, with the material properties varying through the thickness from ceramic to metal at the interface with the stringers. Both types of stringers, rectangular and L-shaped, were assumed to be metallic.

The total stringer depth ($d + w$), was varied from 8 to 16 mm in increments of 2 mm and the angle ratio was 0.8. Two shell aspect ratios, B / A = 0.7 and 1.0, and two length-to-equivalent-radius ratios, $L / R_0 = 1$ and 2, were considered in the analyses. It should be noted that R_0 was 100 mm, Moreover, shell thickness and stringer area index were considered as 1 mm and 20%, respectively. The longitudinal half-wave number was varied from 1 to 30 to identify the corresponding number of half-waves associated with the minimum buckling load of the stiffened shell. The results show that, for small total stringer depths ($d + w = 8$ and 10 mm), buckling generally occurs in the first longitudinal half-wave for both types of stringers, with rectangular stringers providing higher buckling loads. In contrast, for larger values of $d + w$, the rectangular stringers exhibit local buckling, resulting in lower buckling loads than those obtained with L-shaped stringers. For these larger values of $d + w$, the governing longitudinal half-wave number depends on the shell length and reaches 13 and 26 for $L / R_0 = 1$ and 2, respectively, for shells with rectangular stringers. In these cases, the shell aspect ratio (B / A) has minor influence on the buckling load of the stiffened shell because the response is governed by local buckling of the rectangular stringers.

Table 9. Effect of rectangular and L-shaped stringers on buckling load and longitudinal half-wave number of stiffened shells.

		B / A = 1		B / A = 0.7	
$d + w$ (mm)	Stringer type	$L / R_0 = 1$	$L / R_0 = 2$	$L / R_0 = 1$	$L / R_0 = 2$
8	Rectangular	693.497 (1)	610.088 (1) *	564.089 (1)	508.873 (1)
	L-shaped	669.787 (1)	596.826 (1)	542.127 (1)	497.284 (1)
10	Rectangular	694.112 (13)	613.259 (1)	627.889 (1)	513.337 (1)
	L-shaped	726.218 (1)	599.254 (1)	599.412 (1)	500.746 (1)
12	Rectangular	484.498 (13)	431.764 (26)	487.148 (13)	433.721 (26)
	L-shaped	797.676 (1)	608.053 (1)	669.403 (1)	510.050 (1)
14	Rectangular	364.549 (13)	315.959 (26)	365.789 (13)	317.760 (26)
	L-shaped	879.624 (1)	622.718 (1)	747.395 (1)	524.622 (1)
16	Rectangular	289.448 (13)	243.030 (26)	289.371 (13)	244.667 (26)
	L-shaped	968.608 (1)	642.282 (1)	830.118 (1)	544.217 (1)

* Number in the parentheses indicate longitudinal half wave number

5. Conclusions

A survey of the previous studies shows that the buckling of longitudinal stringers (with rectangular cross-sections) is one of the main challenges in designing the stiffened cylindrical shells subjected to axial compression. In this research, conventional longitudinal stiffeners were substituted with L-shaped (angle-shaped) stiffeners to address this issue. Accordingly, a code was written in FORTRAN environment to simulate a longitudinally-stiffened functionally graded elliptical cylindrical shell using semi-analytical finite strip method. The convergence and validity of the model developed in this study were evaluated. The influences of different parameters including L-shaped stiffener geometry, power of functionally graded materials (FGM) and elliptical cylindrical shell properties on the buckling load of the stiffened shell were investigated through a parametric study. A summary of the main results is provided below:

- Conventional stiffeners with rectangular cross-sections lose efficiency when their depths exceed a certain threshold due to excessive slenderness and local buckling.
- L-shaped stiffeners outperform conventional stiffeners, particularly when stiffener total depth is large, by preventing premature local buckling.
- The buckling load of shells stiffened with L-shaped stiffeners is maximized at an optimum angle ratio.
- The optimum angle ratio depends on shell length, stiffener area index, and the number of stiffeners.
- In short shells, L-shaped stiffeners with lower angle ratios (e.g., 0.6) achieve the highest buckling load, while conventional stiffeners provide the lowest performance.
- The significant effect of L-shaped stiffeners on enhancing the buckling load decreases as shell length increases, although their performance remains superior to conventional stiffeners in all cases.
- L-shaped stiffeners with angle ratios below 0.9 can increase the buckling load of elliptical shells by up to approximately 70% within the investigated range of B / A ratios.
- The relative advantage of L-shaped stiffeners over conventional ones is not strongly affected by cross-sectional ovalization or the FGM power index.

From a design perspective, the results indicate that increasing the stiffener depth alone does not necessarily lead to a higher buckling resistance, particularly when local buckling of the stiffener becomes dominant. The L-shaped configuration can provide a more effective use of the stiffener material by delaying local buckling of the web through the restraining effect of the flange. However, excessive web depth or flange width may again promote local instability. Therefore, the stiffener depth and angle ratio should be selected together rather than independently to achieve an effective enhancement of the axial buckling resistance. Despite the comprehensive parametric investigation, this study has some limitations. The present results are based entirely on numerical modelling, and experimental tests on FGM elliptical cylindrical shells with L-shaped stringers were not available for direct validation of the predicted buckling responses and instability modes. In addition, the adopted modelling assumptions may affect the quantitative buckling predictions under practical conditions involving manufacturing imperfections, residual stresses, and material uncertainties. Experimental investigations on representative FGM elliptical shells with L-shaped stringers would therefore be valuable for further validating the predicted buckling loads and local-to-global instability behavior. In addition, a more systematic determination of the optimum angle ratio, stiffener depth, and number of stiffeners could be achieved in future studies by employing appropriate optimization techniques instead of a manual parametric study conducted in this research. Such an optimization framework could also incorporate additional design variables, including stringer thickness, web depth, flange width, and stringer material, to determine the optimum geometry and material properties of L-shaped stringers for a specified shell configuration. Moreover, the results obtained from the present parametric study, or from future optimization-based investigations, could serve as a basis for developing predictive formulations for the buckling load of L-shaped stringer-stiffened shells. In developing such formulations, it is important to distinguish between global shell buckling and local stiffener buckling, since simplified formulations based primarily on shell and stiffener dimensions and material properties may not adequately account for local buckling of the stiffeners.

Author Contributions

D. Poorveis, A. Khajehdezfuly and S. Moradi planned the scheme, initiated the project. D. Poorveis developed the numerical model and examined the theory validation. S.A. Emam conducted parametric studies and calculate the results. The manuscript was written through the contribution of all authors. All authors discussed the results, reviewed, and approved the final version of the manuscript.

Acknowledgments

Not applicable.

Conflict of Interest

The authors declare that they have no conflict of interest.

Funding

This work was supported by Shahid Chamran University of Ahvaz (SCU) [Grant No. SCU.C1404.530].

Data Availability Statements

The data supporting the findings of this study are available from the corresponding author upon reasonable request.

Nomenclature

h	Thickness of shell [mm]
L	Length of shell and stringers [mm]
t	Thickness of L-shaped stiffener [mm]
$d / (d + w)$	Angle ratio
B / A	Ratio of major to minor diameters of ellipse
d	Depth of L-shaped stiffener [mm]
w	Width of L-shaped stiffener [mm]
N_{st}	Number of stringers
N	Power of FGM

References

[1] Semenov, A., Dynamic Buckling of Stiffened Shell Structures with Transverse Shears under Linearly Increasing Load, *Journal of Applied and Computational Mechanics*, 8(4), 2022, 1343-1357.
[2] Shahani, A.R., Kiarasi, F., Numerical and Experimental Investigation on Post-buckling Behavior of Stiffened Cylindrical Shells with Cutout subject to Uniform Axial Compression, *Journal of Applied and Computational Mechanics*, 9(1), 2023, 25-44.
[3] Poorveis, D., Khajehdezfuly, A., Oulapour, M., Aalipour, K., Curvature-guided thickness tailoring for enhanced axial buckling capacity of functionally graded elliptical cylindrical shells, *Mechanics of Advanced Materials and Structures*, 33(1), 2026, 2704685.
[4] Poorveis, D., Khajehdezfuly, A., Oulapour, M., Tamimi, H., Buckling of elliptical cylindrical shell with variable circumferential thickness under fluid lateral pressure, *Journal of Hydraulic Structures*, 12(3), 2026, 1-18.
[5] Poorveis, D., Khajehdezfuly, A., Sardari, M.R., Moradi, S., Interaction of stress distribution and stringer slenderness on buckling of stiffened composite elliptical cylindrical shell under axial compression, *Mechanics Based Design of Structures and Machines*, 54(1), 2026, 2585351.
[6] Moradi, A., Poorveis, D., Khajehdezfuly, A., Buckling of FGM elliptical cylindrical shell under follower lateral pressure, *Steel and Composite Structures*, 45(2), 2022, 175-191.
[7] Khajehdezfuly, A., Poorveis, D., Nazarinia, S., Comparison between linear and nonlinear buckling loads of FGM cylindrical panel with cutout, *International Journal of Non-Linear Mechanics*, 150, 2023, 104361.
[8] Poorveis, D., Khajehdezfuly, A., Moradi, S., Shirshekan, E., A simple spline finite strip for buckling analysis of composite cylindrical panel with cutout, *Latin American Journal of Solids and Structures*, 16(8), 2019, e227.
[9] Mishurenko, N., Semenov, A., Influence of Discretely Introduced Cutouts on the Buckling of Shallow Shells with Double Curvature, *Journal of Applied and Computational Mechanics*, 10(1), 2024, 55-63.
[10] Krause, M., Lyssakow, P., Friedrich, L., Schröder, K.U., Panel buckling of stiffened shell structures with torsional stiff stringer, *Aerospace Science and Technology*, 107, 2020, 106257.
[11] Yaffe, R., Abramovich, H., Dynamic buckling of cylindrical stringer stiffened shells, *Computers & Structures*, 81(8-11), 2003, 1031-1039.
[12] Pasternak, H., Li, Z., Juozapaitis, A., Daniunas, A., Ring stiffened cylindrical shell structures: State-of-the-art review, *Applied Sciences*, 12(22), 2022, 11665.
[13] Ismail, M.S., Purbolaksono, J., Analysis using finite element method of the buckling characteristics of stiffened cylindrical shells, *Australian Journal of Structural Engineering*, 26(4), 2025, 321-331.
[14] Tian, J., Wang, C.M., Swaddiwudhipong, S., Elastic buckling analysis of ring-stiffened cylindrical shells under general pressure loading via the Ritz method, *Thin-Walled Structures*, 35(1), 1999, 1-24.
[15] Barani, S., Poorveis, D., Moradi, S., Buckling analysis of ring-stiffened laminated composite cylindrical shells by Fourier-expansion based differential quadrature method, *Applied Mechanics and Materials*, 225, 2012, 207-212.
[16] Fang, M., Zhu, X., Li, T., Zhang, G., Free vibration characteristics of a finite ring-stiffened elliptic cylindrical shell, *Journal of Vibration and Acoustics*, 139(6), 2017, 061012.
[17] Bai, X., Xu, W., Ren, H., Li, J., Analysis of the influence of stiffness reduction on the load carrying capacity of ring-stiffened cylindrical shell, *Ocean Engineering*, 135, 2017, 52-62.
[18] Li, Z., Pasternak, H., Jäger-Cañás, A., Buckling of ring-stiffened cylindrical shell under axial compression: Experiment and numerical simulation, *Thin-Walled Structures*, 164, 2021, 107888.
[19] Yang, Z., Zhang, X., Pan, G., Xu, Y., Buckling and strength failure for unstiffened and ring-stiffened composite shells, *Ocean Engineering*, 278, 2023, 114513.
[20] Rathinam, N., Prabu, B., Anbazhaghan, N., Buckling analysis of ring stiffened thin cylindrical shell under external pressure, *Journal of Ocean Engineering and Science*, 6(4), 2021, 360-366.
[21] Li, M., Zhang, L., Huang, B., Zhu, H., Fan, H., Multi-failure theory of non-uniformly ring-stiffened composite shells under hydrostatic pressure, *Ocean Engineering*, 299, 2024, 117161.
[22] Zhang, B., Zhao, Y., Zhang, J., Zhang, A., Wan, Z., Experimental and numerical studies on the collapse of Titanium alloy ring-stiffened cylinder, *Engineering Failure Analysis*, 167, 2025, 108928.
[23] Chen, Y., Hu, Z., Zhu, B., Tong, G., Guo, Y., Wang, J., Stability design of axially loaded stringer-stiffened moderately-thick cylindrical shells in steel tubular transmission towers, *Thin-Walled Structures*, 172, 2022, 108874.
[24] Do, Q.T., Muttaqie, T., Park, S.H., Shin, H.K., Cho, S.R., Ultimate strength of intact and dented steel stringer-stiffened cylinders under hydrostatic pressure, *Thin-Walled Structures*, 132, 2018, 442-460.
[25] Kabir, M.Z., Poorveis, D., Buckling of discretely stringer-stiffened composite cylindrical shells under combined axial compression and external pressure, *Scientia Iranica*, 13(2), 2006, 113-123.
[26] Krasovsky, V.L., Kostyrko, V.V., Experimental studying of buckling of stringer cylindrical shells under axial compression, *Thin-Walled Structures*, 45(10-11), 2007, 877-882.
[27] Naghsh, A., Saadatpour, M.M., Azhari, M., Free vibration analysis of stringer stiffened general shells of revolution using a meridional finite strip method, *Thin-Walled Structures*, 94, 2015, 651-662.
[28] Sadeghifar, M., Bagheri, M., Jafari, A.A., Buckling analysis of stringer-stiffened laminated cylindrical shells with nonuniform eccentricity, *Archive of Applied Mechanics*, 81, 2011, 875-886.
[29] Poorveis, D., Khajehdezfuly, A., Sardari, M.R., Moradi, S., An accurate approach for buckling analysis of stringer stiffened laminated composite cylindrical shells under axial compression, *Steel and Composite Structures*, 51(5), 2024, 543-562.
[30] Ghorbanpour Arani, A., Loghman, A., Mosallaie Barzoki, A.A., Kolahchi, R., Elastic buckling analysis of ring and stringer-stiffened cylindrical shells under general pressure and axial compression via the Ritz method, *Journal of Solid Mechanics*, 2(4), 2010, 332-347.
[31] Yu, H., Qiao, P., An efficient compound strip method for buckling analysis of stiffened cylinders, *Thin-Walled Structures*, 198, 2024, 111646.
[32] Shahgholian-Ghahfarokhi, D., Rahimi, G., Buckling load prediction of grid-stiffened composite cylindrical shells using the vibration correlation technique, *Composites Science and Technology*, 167, 2018, 470-481.
[33] Ghahfarokhi, D.S., Rahimi, G., An analytical approach for global buckling of composite sandwich cylindrical shells with lattice cores, *International Journal of Solids and Structures*, 146, 2018, 69-79.
[34] Shahgholian, D., Safarpour, M., Rahimi, A.R., Alibeigloo, A., Buckling analyses of functionally graded graphene-reinforced porous cylindrical shell using the Rayleigh-Ritz method, *Acta Mechanica*, 231(5), 2020, 1887-1902.
[35] Shahgholian-Ghahfarokhi, D., Rahimi, G., Khodadadi, A., Salehipour, H., Afrand, M., Buckling analyses of FG porous nanocomposite cylindrical shells with graphene platelet reinforcement subjected to uniform external lateral pressure, *Mechanics Based Design of Structures and* Machines, 49(7), 2021, 1059-1079.
[36] Rodrigues, F., Vellasco, P.D.S., de Lima, L.R.O., da Silva, A.T., Structural assessment of stainless steel stiffened panels, *Structures*, 57, 2023, 105162.
[37] Elumalai, E.S., Krishnaveni, G., Kumar, R.S., Xavier, D.D., Kavitha, G., Seralathan, S., Hariram, V., Premkumar, T.M., Buckling analysis of stiffened composite curved panels, *Materials Today: Proceedings*, 33(7), 2020, 3604-3611.
[38] Khayat, M., Poorveis, D., Moradi, S., Buckling analysis of laminated composite cylindrical shell subjected to lateral displacement-dependent pressure using semi-analytical finite strip method, *Steel and Composite Structures*, 22(2), 2016, 301-321.
[39] Khayat, M., Poorveis, D., Moradi, S., Hemmati, M., Buckling of thick deep laminated composite shell of revolution under follower forces, *Structural Engineering and Mechanics*, 58(1), 2016, 59-91.
[40] Khayat, M., Poorveis, D., Moradi, S., Buckling analysis of functionally graded truncated conical shells under external displacement-dependent pressure, *Steel and Composite Structures*, 23(1), 2017, 1-16.
[41] Brush, D.O., Almroth, B.O., *Buckling of Bars, Plates, and Shells*, McGraw-Hill, New York, USA, 1975.
[42] Abramovich, H., Weller, T., Singer, J., Effect of sequence of combined loading on buckling of stiffened shells, *Experimental Mechanics*, 28(1), 1988, 1-13.

ORCID iD

Davood Poorveis https://orcid.org/0000-0001-9282-4952
Amin Khajehdezfuly https://orcid.org/0000-0001-9219-003X
Shapour Moradi https://orcid.org/0000-0002-7771-3637
Seyed Ali Emam https://orcid.org/0009-0002-7591-1717

How to cite this article: Poorveis D., Khajehdezfuly A., Moradi S., Emam S.A. L-Shaped Stringer Tailoring to Enhance Axial Buckling of FGM Elliptical Cylindrical Shells, *J. Appl. Comput. Mech.*, xx(x), 2026, 1–20.
https://doi.org/10.22055/jacm.2026.49412.5958